

Response to the editor

Comments to the author:

The revised manuscript has been reviewed again by Referee #2 who acknowledges the revisions to be adequate. Following the recommendations of both referees, I am pleased to accept the paper for publication in ACP subject to technical corrections. See one technical comment by Referee #2. In addition, please specify units for k_{dep} and PBL in Table 1.

Response: Thanks to the editor for handling our manuscript. We have added the units for k_{dep} and PBL in Table 1 of the revised manuscript.

Response to the reviewer

Line 648, JA and CH provided the NO_x emission inventory, while it seems that NO_x emission inventory not used in the studies.

Response: Thanks for the reviewer's comment. We used the NO_x emission inventory and an empirical emission ratio of HONO to NO_x to get the vehicular emissions of HONO in the model simulation. We included a statement in the supplement of the previous version of manuscript. To make it clearer, we have moved this statement to the main text of the revised manuscript (see below).

“We also considered the direct emissions of HONO from vehicles based on a $4 \text{ km} \times 4 \text{ km}$ emission inventory of NO_x and an empirical emission ratio (0.8%) of HONO to NO_x (Kurtenbach et al., 2001; An et al., 2021).”

The authors provide a detailed response and careful revision of the manuscript. I would like to recommend it. In addition, I want to highlight that the level of N_2O_5 is very sensitive to NO, so the constrain of sum NO_x rather than NO and NO_2 maybe under estimate nighttime NO, which lead to the modelled N_2O_5 concentration and its contribution to nitrate represent an upper limit to some extent. This problem cannot be resolved in the work but should take into consideration in future simulations.

Response: We agree that there might be an underestimation of NO during the nighttime when the NO concentration was high. However, we can see from the case study that the O_3 concentration was very low during the NO spikes periods, thus the overestimation of N_2O_5 concentration and its contribution to nitrate might not be significant. We will try to find a better solution to constrain the N_2O_5 simulation in our future studies.

1 **High atmospheric oxidation capacity drives wintertime nitrate pollution in the eastern**
2 **Yangtze River Delta of China**

3

4 Han Zang¹, Yue Zhao^{1,*}, Juntao Huo², Qianbiao Zhao², Qingyan Fu², Yusen Duan^{2,*}, Jingyuan Shao³,
5 Cheng Huang⁴, Jingyu An⁴, Likun Xue⁵, Ziyue Li¹, Chenxi Li¹, Huayun Xiao¹

6

7 ¹School of Environmental Science and Engineering, Shanghai Jiao Tong University, Shanghai, 200240,
8 China

9 ²Shanghai Environmental Monitoring Center, Shanghai 200235, China

10 ³College of Flight Technology, Civil Aviation University of China, Tianjin 300300, China

11 ⁴Shanghai Academy of Environmental Sciences, Shanghai 200233, China

12 ⁵Environment Research Institute, Shandong University, Qingdao, Shandong, 266237, China

13

14 *Correspondence: Yue Zhao (yuezhao20@sjtu.edu.cn); Yusen Duan (duanys@yeah.net)

15

Abstract

Nitrate aerosol plays an increasingly important role in wintertime haze pollution in China. Despite intensive research on the wintertime nitrate chemistry in recent years, quantitative constraints on the formation mechanisms of nitrate aerosol in the Yangtze River Delta (YRD), one of the most developed and densely populated regions in eastern China, remain inadequate. In this study, we identify the major nitrate formation pathways and their key controlling factors during the winter haze pollution period in the eastern YRD using two-year (2018-2019) field observations and detailed observation-constrained model simulations. We find that the high atmospheric oxidation capacity, coupled with high aerosol liquid water content (ALWC), made both the heterogeneous hydrolysis of dinitrogen pentoxide (N_2O_5) and the gas-phase OH oxidation of nitrogen dioxide (NO_2) important pathways for wintertime nitrate formation in this region, with contribution percentages of 69% and 29% in urban areas and 63% and 35% in suburban areas during the haze pollution episodes, respectively. We further find that the gas-to-particle partitioning of nitric acid (HNO_3) was very efficient so that the rate-determining step in the overall formation process of nitrate aerosol was the oxidation of NO_x to HNO_3 through both heterogeneous and gas-phase processes. The atmospheric oxidation capacity (i.e., the availability of O_3 and OH radicals) was the key factor controlling the production rate of HNO_3 from both processes. During the COVID-19 lockdown (January-February 2020), the enhanced atmospheric oxidation capacity greatly promoted the oxidation of NO_x to nitrate and hence weakened the response of nitrate aerosol to the emission reductions in urban areas. Our study sheds light on the detailed formation mechanisms of wintertime nitrate aerosol in the eastern YRD and highlights the demand for the synergetic regulation of atmospheric oxidation capacity and NO_x emissions to mitigate wintertime nitrate and haze pollution in eastern China.

1. Introduction

Atmospheric fine particulate matter (PM_{2.5}) has profound impacts on air quality, climate, and public health (Huang et al., 2014; Wang et al., 2014; Lelieveld et al., 2015; von Schneidemesser et al., 2015). Over the past decades, China has encountered severe PM_{2.5} pollution due to the rapid urbanization and industrialization (Huang et al., 2014; Zhang and Cao, 2015; Tao et al., 2017; Peng et al., 2021). To tackle severe air pollution, Chinese government has implemented active clean air policies such as the “Action Plan for Air Pollution Prevention and Control” in recent years. As a result, anthropogenic emissions of major air pollutants such as sulfur dioxide (SO₂), nitrogen oxides (NO_x), and primary PM have declined dramatically and the nationwide PM_{2.5} air quality have improved significantly (Shao et al., 2018; Zheng et al., 2018; Ding et al., 2019; Zhang et al., 2019). In addition, with the emission reduction of primary PM, secondary aerosol has become the most important component of PM_{2.5} (Shao et al., 2018; Ding et al., 2019; Peng et al., 2021).

Secondary inorganic aerosol consisting mainly of nitrate, sulfate, and ammonium (SNA), contributed to 30-60% of the PM_{2.5} mass in China (Hua et al., 2015; Tao et al., 2017; Ye et al., 2017; Wang et al., 2018; Fu et al., 2020; Lin et al., 2020). During the pollution episodes, the proportion of SNA to PM_{2.5} could exceed 50% (Tao et al., 2017; Liu et al., 2020a; Peng et al., 2021). Before 2013, sulfate was often found to be the most abundant component of PM_{2.5} in Chinese cities (Zhao et al., 2013; Huang et al., 2014; Kong et al., 2014; Xie et al., 2015; Tao et al., 2017). However, with the implementation of stringent clean air policies, anthropogenic emissions of SO₂ in China had dropped by 59% from 2013 to 2017, while NO_x emissions decreased only by 21% during the same period (Zheng et al., 2018). Consequently, sulfate aerosol concentration has decreased dramatically nationwide since 2013, but wintertime nitrate concentration has not decreased much (Ding et al., 2019; Li et al., 2019a; Xu et al., 2019; Fu et al., 2020; Wang et al., 2020b); nitrate has become an increasingly important component of PM_{2.5} in most regions of China during winter (Ye et al., 2017; Yun et al., 2018; Li et al., 2019a; Xu et al., 2019; Chen et al., 2020; Fu et al., 2020; Kong et al., 2020; Lin et al., 2020; Xie et al., 2020; Zhai et al., 2021; Zhang et al., 2021). The high loading of nitrate has been considered playing an important role in winter haze pollution (Wen et al., 2015; Sun et al., 2018). Therefore, identifying the major nitrate formation pathways and their controlling factors during haze events is of great importance for developing effective particulate pollution mitigation policies in China.

In polluted regions, the nitrate aerosol arises mainly from two pathways: (1) the gas-phase oxidation of nitrogen dioxide (NO₂) by OH radicals producing nitric acid (HNO₃) (Calvert and Stockwell, 1983) and (2) the heterogeneous hydrolysis of dinitrogen pentoxide (N₂O₅) that was produced from the reaction of NO₂ with nitrate (NO₃) radicals, on aqueous aerosols (Bertram and Thornton, 2009; Bertram et al., 2009; Wagner et al., 2013; McDuffie et al., 2019). The gas-phase OH + NO₂ pathway primarily occurs during the daytime and is mainly influenced by the atmospheric oxidation capacity despite the NO₂ concentration (Chen et al., 2020; Fu et al., 2020). The heterogeneous formation of nitrate via N₂O₅ hydrolysis is greatly affected by aerosol liquid water content (ALWC) and the

production of N_2O_5 (Alexander et al., 2020; Lin et al., 2020; Wang et al., 2020b). As a result, this heterogeneous pathway is generally weak during the daytime because of the fast photolysis of NO_3 radicals and titration by NO (Wayne et al., 1991; Brown and Stutz, 2012), which inhibit N_2O_5 production. However, it could be the dominant pathway for nitrate formation during the nighttime (Wang et al., 2017; McDuffie et al., 2019), where N_2O_5 can be produced more efficiently and its hydrolysis is favored by the high relative humidity (or ALWC).

There have been a number of field studies on the pollution characteristics and formation mechanisms of nitrate aerosol during haze events in China over the past decades (Tao et al., 2016; Li et al., 2018; Sun et al., 2018; Wen et al., 2018; Ding et al., 2019; Ye et al., 2019; Chen et al., 2020; Fu et al., 2020; Lin et al., 2020; Wang et al., 2020b; Zhao et al., 2020a; Chan et al., 2021). However, most of these studies were carried out in the North China Plain (NCP) (Li et al., 2018; Wen et al., 2018; Chen et al., 2020; Fu et al., 2020; Wang et al., 2020b; Chan et al., 2021). Earlier studies suggested that the nitrate formation during the pollution episodes in this region was mainly attributed to the heterogeneous hydrolysis of N_2O_5 (Su et al., 2017; Wang et al., 2017; He et al., 2018; Li et al., 2018). However, recent studies showed that the gas-phase $\text{OH} + \text{NO}_2$ process has become more important, and sometimes this process was even the dominant pathway for nitrate formation (Chen et al., 2020; Fu et al., 2020). The Yangtze River Delta (YRD) in eastern China is one of the most developed regions in China (Ding et al., 2013). The wintertime O_3 concentration is relatively high in this region, with an average of ~ 20 ppb, and sometimes could even reach 75 ppb (Li et al., 2019c; Ye et al., 2019; Zhao et al., 2020a), which is significantly higher than that (average: 6-16 ppb) in the NCP region (Li et al., 2019a; Duan et al., 2020; Liu et al., 2020a). Furthermore, the relative humidity (RH) in this region is also high, with the average winter RH ranging from 63% to 71% (Tao et al., 2016; Shen et al., 2020; Yu et al., 2020b), which was also significantly higher than the average RH (20-40%) in the NCP region (Fang et al., 2019; Li et al., 2019a; Huang et al., 2020; Xie et al., 2020). The high atmospheric oxidation capacity, coupled with the high RH that led to high ALWC, would favor the production of secondary aerosol (Peng et al., 2021).

Haze pollution events frequently occurred in the YRD during winter (Hua et al., 2015; Sun et al., 2018; Ding et al., 2019). Although there have been many studies on the pollution characteristics of nitrate and $\text{PM}_{2.5}$ in this region (Tao et al., 2016; Sun et al., 2018; Chen et al., 2019; Ding et al., 2019; Ye et al., 2019; Lin et al., 2020; Shen et al., 2020), only a few studies have focused on the nitrate formation mechanisms. It has been reported that the heterogeneous hydrolysis of N_2O_5 contributed dominantly to nitrate formation in the western YRD (Sun et al., 2018), and its production rate could be 5 times higher than that of the gas-phase $\text{OH} + \text{NO}_2$ process during severe haze pollution events (Lin et al., 2020). In contrast, some other studies have qualitatively pointed out that the gas-phase $\text{OH} + \text{NO}_2$ reaction was an important formation pathway of nitrate in the eastern YRD, though the heterogeneous hydrolysis of N_2O_5 during the nighttime also contributed (Ye et al., 2019; Zhao et al., 2020a). Overall, quantitative constraints on the detailed formation mechanisms of wintertime nitrate aerosol in the YRD region remain limited. The relative

contribution of different nitrate formation pathways and their controlling factors are still unclear.

In this study, we conducted hourly measurements of nitrate and associated particulate and gaseous air pollutants at an urban site and a regional site in the eastern YRD during winter in 2018 and 2019, aiming to clarify the nitrate formation mechanisms during winter. An observation-constrained box model using the detailed Master Chemical Mechanism (MCM v3.3.1) updated with the state-of-the-art heterogeneous chemistry of N_2O_5 , NO_2 , and particulate nitrate was employed to quantitatively identify the major reaction pathways and key controlling factors for wintertime nitrate aerosol formation in this region. This study will help to understand the nitrate aerosol chemistry in the eastern YRD and develop effective strategies to mitigate secondary aerosol pollution in this densely populated region.

2. Materials and methods

2.1 Observation sites and instrumentation

$\text{PM}_{2.5}$ and its chemical composition, inorganic gases, volatile organic compounds (VOCs), and meteorological parameters were continuously measured at a regional site (Qingpu) and an urban site (Pudong) in Shanghai from December 1 to February 12 in both 2018 and 2019. The Qingpu site (120.989°E , 31.097°W) is a suburban site (see Fig. 1), located near the Dianshan Lake and surrounded by the residential areas and vegetation, and about 46 km away from the urban Shanghai. Besides, the Qingpu site is located at the junction of Shanghai, Jiangsu, and Zhejiang province and is a typical regional site in the eastern YRD. The instruments at this site were on the rooftop of a 10 m tall building. The Pudong site (121.533°E , 31.228°W) is an urban site located near the Century Avenue with heavy traffic, and it is only ~ 3 km from the business center Lujiazui. The instruments at this site were located on the roof of a 20 m tall building. The eastern YRD region is affected by the subtropical monsoon climate, dominated by the northwest and northeast winds in winter.

The measurements at the two sites were conducted hourly. The $\text{PM}_{2.5}$ mass concentration was measured by a Tapered Element Oscillating Microbalance combined with Filter Dynamic Measurement System (TEOM-FDMS, TEOM 1405-F, Thermo Fisher Scientific, USA.). Water-soluble ions including NO_3^- , SO_4^{2-} , NH_4^+ , Cl^- , Na^+ , Ca^{2+} , and Mg^{2+} were measured using an online Monitor for Aerosol and Gases (MARGA, ADI 2080, Applikon Analytical B.B.Corp., Netherlands). Organic carbon (OC) and elemental carbon (EC) were measured by a semi-continuous OC/EC analyzer (Model 4, Sunset Laboratory Inc., USA), and a denuder was installed before analyzer to avoid the disturbance of organic vapors. The surface area and volume concentrations of aerosol particles were measured using a scanning mobility particle sizer (SMPS, TSI, USA, which consists of a 3080 electrostatic classifier, a 3081A differential mobility analyzer, and a 3787 condensation particle counter) and an aerodynamic particle sizer (APS 3321, TSI, USA). The combination of SMPS and APS was able to cover the particle size range from 13.6 nm to 10 μm . Considering that the Pudong sampling site lacks the data of aerosol volume and surface area concentrations, we performed a linear fit between the aerosol surface/volume and $\text{PM}_{2.5}$ mass concentration at the

Qingpu site (see Figure S1 in the supplement), and predicted the values for the Pudong site based on such a linear fit and the measured PM_{2.5} mass concentration. The surface/volume concentrations of dry aerosol particles measured by SMPS and APS were corrected to the ambient RH based on an empirical composition-kappa function and the kappa-Köhler function (see details in Section S1 of the Supplement). The O₃, NO_x, and SO₂ were measured by an Ozone, NO_x, and SO₂ analyzer (Model 49i, 42i, and 43i, Thermo Fisher Scientific, USA), respectively. A total of 56 VOCs were measured using gas chromatography equipped with a flame ionization detector (GC-FID, Chromatotec A11000/A21022 at the Qingpu site and PerkinElmer Clarus 580 at the Pudong site). Meteorological parameters including temperature, RH, pressure, wind speed and direction were measured by a meteorological transducer (WXT520, Vaisala Ltd., Finland).

2.2 Estimation of aerosol liquid water content and pH

The ISORROPIA-II thermodynamic model was used to calculate aerosol pH and ALWC (Fountoukis and Nenes, 2007). The water-soluble inorganic ion concentrations, along with RH and temperature, were used as the model input. The model was run in the forward mode, which would give a more accurate estimation of aerosol pH than using the reverse mode with only particulate inorganic ions as the model input (Guo et al., 2015; Hennigan et al., 2015). Besides, considering the relatively high RH in eastern YRD, we selected the metastable state for aerosol in this study. ISORROPIA-II calculated the equilibrium concentrations of particle hydronium ions (H_{aq}⁺, μg m⁻³) and ALWC (μg m⁻³) in per air volume. Then the aerosol pH can be derived by the following equation:

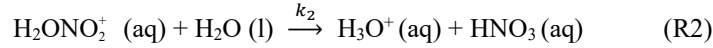
$$\text{pH} = -\log_{10}(\text{H}_{\text{aq}}^+) = -\log_{10}\frac{1000\text{H}_{\text{air}}^+}{\text{ALWC}} \quad (1)$$

Where H_{aq}⁺ is the concentration of hydronium ions in aqueous aerosol (mol L⁻¹). It should be mentioned that when the RH was extremely high (> 95%), a slight deviation in measured RH would cause significant uncertainty in the estimation of ALWC. Therefore, we only considered the data with the RH below 95% in the further analysis.

2.3 Observation-constrained model simulation

The Framework for 0-D Atmospheric Modeling (F0AM v3.1) (Wolfe et al., 2016) employing the MCM v3.3.1 (Jenkin et al., 2015) was used to simulate the formation of nitrate in the pollution events during the whole observation period. Figure 2 summarizes the formation pathways of HNO₃ in the atmosphere (Alexander et al., 2020; Chan et al., 2021). In the model, we considered the reaction pathways including heterogeneous hydrolysis of N₂O₅ (R3) and NO₂ (R8), gas-phase OH + NO₂ (R7), NO₃ radical oxidation of VOCs (R5), and reaction of NO with hydroperoxy (HO₂) radicals (R2), which together contributed to 88% of HNO₃ formation in the global troposphere (Alexander et al., 2020). The model did not include the hydrolysis of NO₃ radicals and organic nitrate (R1, R4, and R6), as well as the reaction of NO₂ with halogen oxide species (R9). However, these pathways only had a small contribution to the production of HNO₃ (Alexander et al., 2020). Therefore, they would not significantly affect the model results in this study.

The default MCMv3.3.1 does not consider the heterogeneous hydrolysis of N₂O₅ in detail and the heterogeneous production of nitrous acid (HONO), an important precursor of OH radicals in the polluted atmosphere. Therefore, we parameterized these processes in the model based on recent advances in these processes. For the heterogeneous hydrolysis of N₂O₅, the N₂O₅ molecules accommodated on aqueous aerosols can undergo reversible hydrolysis to form NO₃⁻ and H₂ONO₂⁺ (R1), followed by the reaction of H₂ONO₂⁺ with H₂O or Cl⁻ to form HNO₃ or nitryl chloride (ClNO₂) (R2 and R3) (Finlayson-Pitts et al., 1989; Schweitzer et al., 1998; Thornton and Abbatt, 2005):



The rate of the heterogeneous hydrolysis of N₂O₅ on aqueous aerosols (k_4) could be calculated by eq. 2 when ignoring the gas-phase diffusion limitation:

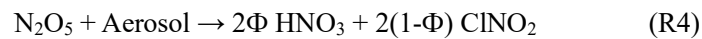
$$k_4 = \frac{\gamma \text{N}_2\text{O}_5 \cdot c \cdot S_a}{4} \quad (2)$$

where $\gamma\text{N}_2\text{O}_5$ is the uptake coefficient of N₂O₅, defined as the probability of removal of N₂O₅ per collision with the wet aerosol surface; c is the mean molecular speed of N₂O₅; S_a is the measured aerosol surface area concentration. In this study, we employed an observation-based empirical parameterization of $\gamma\text{N}_2\text{O}_5$, which provided a reasonable representation of the PM_{2.5} reactivity toward N₂O₅ at different Chinese sites, according to a recent study (Yu et al., 2020a):

$$\gamma\text{N}_2\text{O}_5 = \frac{4}{c} \frac{V_a}{S_a} K_H \times k_{1f} \times \left(1 - \frac{1}{\left(\frac{k_2}{k_{1b}} \times \frac{[\text{H}_2\text{O}]}{[\text{NO}_3^-]} \right) + 1 + \left(\frac{k_3}{k_{1b}} \times \frac{[\text{Cl}^-]}{[\text{NO}_3^-]} \right)} \right) \quad (3)$$

where V_a is the measured aerosol volume concentration; K_H is the Henry's law coefficient of N₂O₅, with a value of 51 M atm⁻¹ (Bertram and Thornton, 2009); k_{1f} is the second-order reaction rate constant of N₂O₅ with water, which was calculated using a linear function with [H₂O], as $3.0 \times 10^4 \times [\text{H}_2\text{O}]$ (Yu et al., 2020a); $\frac{k_2}{k_{1b}}$ and $\frac{k_3}{k_{1b}}$ are the relative rates of reactions of H₂ONO₂⁺(aq) with H₂O or Cl⁻ (R2 and R3) versus that with NO₃⁻ (the reverse reaction of R1), with values determined to be 0.033 and 3.4, respectively (Yu et al., 2020a); and [H₂O], [NO₃⁻], and [Cl⁻] are the molarity of water, nitrate, and chloride in aerosol, respectively.

The yields (Φ , ranging between 0 and 1) of HNO₃ and ClNO₂ from the heterogeneous hydrolysis of N₂O₅ depend on the H₂O and Cl⁻ content in the aerosol (Bertram and Thornton, 2009; Yu et al., 2020a). In this study, the yield of HNO₃ (Φ_{HNO_3}) was estimated from eq. 4 (Bertram and Thornton, 2009; Yu et al., 2020a):



$$\Phi_{HNO_3} = 1 - 1 / (1 + \frac{[H_2O]}{\frac{k_3}{k_2} \times [Cl^-]}) \quad (4)$$

where $\frac{k_3}{k_2}$ is the ratio of reaction rates of R3 versus R2, which has been determined to be 105 (Bertram and Thornton, 2009; Yu et al., 2020a).

Photolysis of HONO was shown to contribute 20-92% of the production of OH radicals during winter haze pollution events in China (Tan et al., 2017; Slater et al., 2020; Xue et al., 2020). Here, on the basis of previous studies (Lee and Schwartz, 1983; Kleffmann et al., 1998; Kurtenbach et al., 2001; Wong et al., 2011; Wong et al., 2013; Han et al., 2016; Ye et al., 2016; Liu et al., 2017; Trinh et al., 2017; Romer et al., 2018; Zare et al., 2018; Liu et al., 2019; Wang et al., 2020a; Xue et al., 2020), we parameterized the major heterogeneous production pathways of HONO and its dry deposition to estimate the HONO budget during the pollution episodes. We also considered the direct emissions of HONO from vehicles based on a 4 km × 4 km emission inventory of NO_x and an empirical emission ratio (0.8%) of HONO to NO_x (Kurtenbach et al., 2001; An et al., 2021). The added mechanisms are summarized in Table 1. A detailed description of the parameterization is provided in the Supplement (Section S2). Considering that there remain significant uncertainties in the key parameters (i.e., the uptake coefficient of NO₂ on aerosol or ground surfaces, EF, and HONO emission ratios) of the heterogeneous HONO formation pathways and its direct emissions as listed in Table 1, we performed the sensitivity analyses for these parameters to evaluate their influences on the model results.

In addition, we considered the dilution of species via deposition, entrainment, etc. using a highly simplified parameterization:

$$\frac{d[X]}{dt} = -k_{dil} ([X] - [X]_{bkg}) \quad (5)$$

where k_{dil} is the first-order dilution rate constant; $[X]_{bkg}$ is a fixed background concentration of pollutants. Here, a typical dilution lifetime of one day was assumed, i.e., $k_{dil} = 1/24 \text{ h}^{-1}$. As the species background concentration was unknown, $[X]_{bkg}$ was set to 0 for simplicity. Considering the uncertainties in the parameterization of dilution process using a constant rate constant, we also conducted a sensitivity test for k_{dil} with its value ranging between 0.028 h^{-1} and 0.2 h^{-1} , which covers the typical values used in box model simulations (Romer et al., 2018; McDuffie et al., 2019; Liu et al., 2020b), to evaluate its influence on the model results.

In the model, the j values of various gaseous species were calculated using the default MCMv3.3.1 parameterization with input of the solar zenith angle at the observations sites and scaled by the ratio of measured to calculated $j\text{NO}_2$ values. The observed pollutant concentrations and meteorological parameters were used as the model input, which were updated hourly (one model step) using the observation data and held constant during each model step, except for the observed concentrations of NO and NO₂ (the sum of NO and NO₂ concentrations was constrained by the observation, but

their specific ratios were simulated by the model).

3. Results and Discussion

3.1 Overview of pollution characteristics during winter

Table 2 shows the overall pollution conditions of the two observation sites in winter 2018 and 2019. The average $PM_{2.5}$ concentration increased by 17-21% in 2019 compared to that in 2018. Accordingly, nitrate concentration also increased by 11-14% in 2019. The O_3 concentration was slightly higher in 2019 than in 2018, consistent with increased atmospheric oxidation capacity in recent years (Lu et al., 2018; Li et al., 2019b; Liu and Wang, 2020; Yang et al., 2020). In the two years, both of the $PM_{2.5}$ and nitrate concentrations at the Qingpu site were higher than those at the Pudong site. As mentioned above, the Qingpu site is at the junction of Shanghai, Jiangsu, and Zhejiang, so it is more easily influenced by the transport of air pollutants from Jiangsu, which is usually more polluted than Shanghai. Besides, the average temperature at the Qingpu site was also slightly lower than that at the Pudong site, which might to some extent favor the gas-to-particle partitioning of HNO_3 . Notably, the average RH was as high as 80% during the observation period, which was significantly higher than that (63%) recorded in 2016 (Tao et al., 2016). In particular, the RH exceeded 90% for more than one third of the days during the observation period.

Taking the Pudong site in 2019 as an example, we analyzed the time series of $PM_{2.5}$, nitrate, and other related parameters and presented the results in Figure 3 (Time series of the pollutants at the Qingpu site can be seen in Section S3 and Figure S2). $PM_{2.5}$ pollution events occurred frequently in the eastern YRD during winter. During the observation period, the $PM_{2.5}$ concentration exceeded $75 \mu g m^{-3}$ for 34 days and $150 \mu g m^{-3}$ for 6 days. During the pollution episodes ($PM_{2.5} > 75 \mu g m^{-3}$), nitrate had become the most important component of $PM_{2.5}$, and its concentration was a factor of 2.2 higher than that of sulfate. In winter, the emission of NO_x was obviously high. During the periods with high nitrate concentration, the NO_x concentration always exceeded 100 ppb. The O_3 concentration was also at a relatively high level, with a maximum value of 60 ppb and an average of 22 ppb, which was much higher than the wintertime average O_3 concentration (6-16 ppb) in the NCP (Li et al., 2019a; Duan et al., 2020; Liu et al., 2020a). The concentration of odd oxygen ($O_x = O_3 + NO_2$) ranged between 20-83 ppb with an average of 44 ppb, indicating a relatively high atmospheric oxidation capacity in the eastern YRD during winter. Consistently, the nitrogen oxidation ratio (NOR, $NOR = NO_3 / (NO_3 + NO_2)$) was up to 0.51, suggesting a high degree of atmospheric oxidation. Meanwhile, the high atmospheric RH in the eastern YRD led to a high ALWC. During the high nitrate periods, the ALWC was often at its peak and could exceed $200 \mu g m^{-3}$ on rainy or haze-foggy days. Such a high ALWC level would have an important impact on the nitrate formation. Notably, the NO_x concentration dropped sharply on 23 January and kept at a low level until the end of the observation (12 February, 2020). This is mainly a result of marked emission reductions during the COVID-19 lockdown. Such an emission reduction had a complicated influence on the nitrate formation chemistry, which will be discussed in detail in Section 3.5.

Figure 4 shows the mass ratio of nitrate to $\text{PM}_{2.5}$ as a function of the $\text{PM}_{2.5}$ concentration and ALWC at Qingpu and Pudong sites in 2018 and 2019. The ratio of nitrate to $\text{PM}_{2.5}$ increased with increasing $\text{PM}_{2.5}$ concentration. When the $\text{PM}_{2.5}$ concentration was above $75 \mu\text{g m}^{-3}$, the average mass fraction of nitrate was more than 30%. In addition, the nitrate formation rate was much higher than that of sulfate and ammonium during $\text{PM}_{2.5}$ pollution episodes, as indicated by the slope of nitrate vs. $\text{PM}_{2.5}$ that was twice that of the other two ions (see Figure S3). These results indicate that the formation of nitrate played a driving role in the formation of $\text{PM}_{2.5}$ pollution. In general, when the ALWC was high, the nitrate concentration was also at a high level. On one hand, ALWC could promote the nitrate formation by favoring the heterogeneous hydrolysis of N_2O_5 and the gas-to-particle partitioning of HNO_3 . On the other hand, the increase in nitrate concentration could enhance the hygroscopicity of $\text{PM}_{2.5}$, leading to an increase in ALWC, which would further promote the nitrate formation (Wang et al., 2020b). It is worth noting that, when $\text{PM}_{2.5} < 100 \mu\text{g m}^{-3}$, the mass ratio of NO_3^- to $\text{PM}_{2.5}$ increased rapidly with rising $\text{PM}_{2.5}$ concentration, but when the $\text{PM}_{2.5}$ concentration exceeded $100 \mu\text{g m}^{-3}$, the ratio reached a plateau. This might be due to the fact that when the $\text{PM}_{2.5}$ concentration increased to a certain level, the formation process of other components may also speed up, causing the nitrate proportion to stay basically constant.

3.2 Gas-to-particle partitioning of nitrate

The gas-to-particle partitioning of nitrate determines the sensitivity of particulate nitrate formation to the production of HNO_3 . Figure 5 shows the particulate nitrate concentration (measured) and its fraction to total nitrate (ϵHNO_3 , $\epsilon\text{HNO}_3 = \text{NO}_3^-/(\text{NO}_3^- + \text{HNO}_3)$), predicted by ISORROPIA-II) as a function of ALWC and aerosol pH. In order to avoid the influence of rainy and foggy days during the observation period which could lead to the abnormal high ALWC, we only used the data with RH below 95% for analysis. Obviously, ALWC promoted the formation of particulate nitrate, but such a promoting effect varied greatly under different aerosol pH (top panel in Figures 5a-d). As the pH increased, the slope of nitrate vs. ALWC also increased significantly, indicating a stronger promoting effect. ALWC plays a dual role in the formation of nitrate aerosol: it can promote the heterogeneous formation of nitrate, e.g., via N_2O_5 hydrolysis, by providing more reaction medium and decreasing the kinetic limitation (Mozurkewich and Calvert, 1988; Bertram and Thornton, 2009; Wang et al., 2020b); the ALWC can also promote the gas-to-particle partitioning of HNO_3 . The different promoting effect of ALWC under different aerosol pH is mainly due to the fact that pH can significantly influence the gas-to-particle partitioning of HNO_3 . As shown in Figures 5a-d (bottom panel), when the aerosol pH was low, the gas-to-particle partitioning of HNO_3 was inhibited, with the value of ϵHNO_3 basically below 0.6 at $\text{pH} < 2$. Under these conditions, the increase of particulate nitrate concentration would require more ALWC. When the pH increased, the inhibition effect of pH on the gas-to-particle partitioning of HNO_3 was weakened. When the pH was higher than 2.5, the nitrate was almost in the particle phase ($\epsilon\text{HNO}_3=1$). As a result, the increase of ALWC would rapidly promote the nitrate formation, particularly when ALWC was at a low level. It is important to point out that during the whole observation period, the values of ϵHNO_3 were larger than 0.9 for 90% of time when the $\text{PM}_{2.5}$ concentration was higher than $75 \mu\text{g m}^{-3}$ (see Figure S4). This indicates

that the gas-to-particle partitioning of HNO_3 was very efficient and not a limiting factor for particulate nitrate formation during the pollution episodes. The gas-to-particle partitioning of HNO_3 was also efficient in the NCP region, and its average ϵ_{HNO_3} could reach 100% during the haze pollution period (Guo et al., 2018; Li et al., 2019a). However, the average ϵ_{HNO_3} in the northeastern United States during winter was only 39% (Guo et al., 2018), this might be due to the relatively lower pH in this region (0.8 ± 1.0) (Guo et al., 2016), which inhibited the gas-to-particle partitioning.

3.3 Observational constraints on the nitrate formation mechanism

The dominant nitrate formation pathway is different during the different time of a day. The heterogeneous hydrolysis of N_2O_5 was often found to be an important pathway for nighttime nitrate formation. Here, we evaluated the role of this pathway to nitrate formation in the eastern YRD using the nighttime averages correlation between particulate nitrate concentration and the production of N_2O_5 . Due to the lack of direct observational data of N_2O_5 in this study, we used the value of square of NO_2 multiplied by O_3 ($[\text{NO}_2]^2 \times \text{O}_3$) to indicate the N_2O_5 level (Liu et al., 2020a). Figure 6 shows the nighttime average nitrate concentration as a function of $[\text{NO}_2]^2 \times \text{O}_3$ in winter. The average particulate nitrate concentration showed a strong positive correlation with $[\text{NO}_2]^2 \times \text{O}_3$. In particular in 2019, as the value of $[\text{NO}_2]^2 \times \text{O}_3$ increased to $\sim 15000 \text{ ppb}^3$, the nitrate concentration increased from $15\text{--}20 \mu\text{g m}^{-3}$ to $40\text{--}45 \mu\text{g m}^{-3}$, suggesting that the heterogeneous hydrolysis of N_2O_5 was an important pathway for wintertime nitrate formation in the eastern YRD. Notably, there are some data points with low values of $[\text{NO}_2]^2 \times \text{O}_3$ but high nitrate concentrations. This might be partly due to their relatively high aerosol pH (> 3), which could promote the gas-to-particle partitioning of HNO_3 .

To evaluate the role of the gas-phase $\text{OH} + \text{NO}_2$ process in nitrate formation during the daytime, we use the O_x to indicate the atmospheric oxidation capacity due to the lack of direct observational data of OH radicals. Figure 7 shows the daytime average particulate nitrate concentration as a function of O_x . Notably, as the O_x concentration increased, the nitrate concentration also increased significantly. However, the increase in ALWC seemed to have a relatively small impact on the nitrate concentration during the daytime, indicating that the reaction of NO_2 with OH radicals to form HNO_3 (rather than the gas-to-particle partitioning) was a rate-limiting step in daytime nitrate formation. We also note that there are some data points with low O_x values but high ALWC and nitrate concentrations (Figure 7c). This phenomenon might be owing to a certain degree of heterogeneous process in the haze-foggy days, when the photochemical reactions were relatively weak. Overall, the high atmospheric oxidation capacity made the gas-phase $\text{OH} + \text{NO}_2$ reaction an important pathway for nitrate formation during the daytime in the eastern YRD.

3.4 Model constraints on the nitrate formation mechanism

To quantify the contribution of different formation mechanisms to wintertime nitrate formation in the eastern YRD, we used an observation-constrained model (F0AM v3.1) updated with the heterogeneous chemistry of N_2O_5 and NO_2 (see Section 2.3 for details) to simulate the formation

rate of HNO_3 from different pathways during the observation period. During the winter of 2019, six haze pollution episodes ($\text{PM}_{2.5} > 75 \mu\text{g m}^{-3}$) occurred at both sites (there was an additional episode during the outbreak of COVID-19 epidemic, which was discussed separately in Section 3.5). We conducted simulations for all the six pollution episodes and took two representative ones at the Pudong site for the detailed analysis. Considering the large uncertainties in ALWC estimation and aerosol surface area/volume correction at high RH levels ($> 95\%$), which could significantly affect the simulation results, we excluded the simulated data above 95% RH from the further analysis. Figure 8 shows the time series of various particulate (measured) and gaseous (measured and simulated) air pollutants, as well as the formation rate of HNO_3 (simulated) from different pathways during these two episodes (The case studies of the same episodes at the Qingpu site are given in Section S4 and Figure S5).

In episode 1 (Figure 8a), the nitrate concentration increased rapidly from $15.2 \mu\text{g m}^{-3}$ at 22:00 on 29 December to $39.0 \mu\text{g m}^{-3}$ at 10:00 on 30 December, with an average growth rate of $2.0 \mu\text{g m}^{-3} \text{ h}^{-1}$. The simulated NO_2 concentration was in good agreement with the observation, except for a short period around the midnight of 30 December, during which the NO emissions led to an over-prediction of the NO_2 level. During the high nitrate periods, the nighttime N_2O_5 concentration could reach 0.5-1 ppb and contributed noticeably to HNO_3 formation via the heterogeneous hydrolysis. However, the high daytime OH concentration (up to $2.5 \times 10^6 \text{ molecules cm}^{-3}$) facilitated a relatively more rapid nitrate formation from the gas-phase $\text{OH} + \text{NO}_2$ pathway. The average production rate of HNO_3 from the gas-phase $\text{OH} + \text{NO}_2$ reaction during the daytime was $2.9 \mu\text{g m}^{-3} \text{ h}^{-1}$, which was twice the average production rate of HNO_3 from the heterogeneous hydrolysis of N_2O_5 during the nighttime.

We note that the overestimation of NO_2 during the night of 30 December (case 1) could lead to an overestimation of nighttime HONO, but it did not significantly affect the overall production rate of HONO and thereby OH radicals in this case, which was dominated by the daytime heterogeneous photochemical processes (see Figure S7, HONO production rate in the base scenario). In addition, as the O_3 concentration in the model was constrained by the measured value, which was very low ($< 5 \text{ ppb}$) during this time, the overestimation of NO_2 would also not significantly affect the prediction of N_2O_5 . As a result, the over-prediction of NO_2 would not have a large influence on the major formation pathways of nitrate.

There were two cases in the episode 2 (Figure 8b). In case 2, the concentration of nitrate increased from $26.8 \mu\text{g m}^{-3}$ at 05:00 to $46.0 \mu\text{g m}^{-3}$ at 13:00 on 12 January, 2020, with an average growth rate of $2.4 \mu\text{g m}^{-3} \text{ h}^{-1}$. Then, the nitrate concentration achieved a fast growth from 40.2 to $70.5 \mu\text{g m}^{-3}$ within only six hours during the night of 12 January, with an average rate of $5.1 \mu\text{g m}^{-3} \text{ h}^{-1}$. During the nitrate increasing period, the maximum OH concentration was $\sim 1.0 \times 10^6 \text{ molecules cm}^{-3}$. As a result, the gas-phase $\text{OH} + \text{NO}_2$ reaction led to a slow increase of nitrate concentration in the daytime of 12 January. During the nighttime, the N_2O_5 concentration quickly increased to 0.83 ppb. The high

N₂O₅ level, in combination with the high ALWC, made the heterogeneous hydrolysis of N₂O₅ a more important pathway for nitrate formation. The simulated average production rate of HNO₃ from the heterogeneous hydrolysis of N₂O₅ during this case was 4.0 μg m⁻³ h⁻¹, which was 3.6 times that of the formation rate from the gas-phase OH + NO₂ reaction (1.1 μg m⁻³ h⁻¹). In case 3, the nitrate concentration increased from 22.5 μg m⁻³ at 0:00 to 53.8 μg m⁻³ at 11:00 on 14 January, with an average growth rate of 2.8 μg m⁻³ h⁻¹. The N₂O₅ concentration was at a high level (~ 1 ppb) during the nighttime and its hydrolysis contributed significantly to nitrate formation at the beginning of the nitrate-increasing period. In the morning of 14 January, the OH concentration rapidly increased to 1.3 × 10⁶ molecules cm⁻³, resulting in considerable nitrate formation from the gas-phase process. The average production rates of HNO₃ from the heterogeneous and gas-phase processes in this case were 3.9 and 2.4 μg m⁻³ h⁻¹, respectively, suggesting that both processes were important nitrate formation pathways.

As mentioned above, there were six haze pollution episodes during the observation period. At the Qingpu site, the heterogeneous hydrolysis of N₂O₅ was the major formation pathway (65-80%) of nitrate aerosol for four episodes, while the gas-phase OH + NO₂ reaction had a major contribution (54-60%) for the other two episodes. At the Pudong site, the heterogeneous process also contributed dominantly (67-89%) to nitrate formation during four episodes, and for the other two episodes, the contributions of the heterogeneous and gas-phase processes were comparable (51-53% vs. 45-47%). Figure S6 shows the average diurnal variation of the production rates of HNO₃ from different pathways during the observation period in 2019. The gas-phase process produced HNO₃ mainly from 7:00 to 16:00, while the HNO₃ production from the heterogeneous process occurred mainly from 17:00 to 6:00. The average production rates of HNO₃ from the heterogeneous and gas-phase processes are given in Figure 9. At the Qingpu site, the average production rate of HNO₃ from the two processes was 3.79 μg m⁻³ h⁻¹ for the heterogeneous process during the nighttime (14 hours) vs. 2.94 μg m⁻³ h⁻¹ for the gas-phase reaction during the daytime (10 hours). The production rate from other processes such as NO₂ hydrolysis and NO₃ radical oxidation of VOCs was only 0.08 μg m⁻³ h⁻¹. Therefore, the heterogeneous and gas-phase processes contributed to 63% and 35% of nitrate formation at this site, respectively. At the Pudong site, the average formation rate of HNO₃ from the hydrolysis of N₂O₅ was 3.83 μg m⁻³ h⁻¹, significantly higher than that from the gas-phase reaction (2.27 μg m⁻³ h⁻¹). As a result, the contributions of heterogeneous and gas-phase processes to nitrate formation were 69% and 29%, respectively.

As mentioned in Section 2.3, significant uncertainties remain in the key parameters of the heterogeneous HONO formation pathways and the dilution process in the model, which could affect the prediction of OH radicals and N₂O₅ and thereby the production of HNO₃. However, sensitive analyses for various parameters show that the current parameterization of the heterogeneous HONO formation and dilution process in the model allows for robust quantitative constraints on the relative contributions of the gas-phase and heterogeneous processes to nitrate formation during haze pollution episodes (see Section S5 and Figures S7, S8 for more details). In addition, monoterpenes

that are very reactive to NO_3 radicals (Atkinson and Arey, 2003) were not included in the model, because their measurements are not available in this study. However, a case study considering the monoterpene chemistry in the model shows that the low monoterpene emissions during the winter did not significantly affect the budget of NO_3 radical and N_2O_5 and thereby the nighttime HNO_3 production (see Section S6 and Figure S9 for more details).

As discussed in Section 3.2, the gas-to-particle partitioning of HNO_3 was rather efficient, with the value of $\varepsilon_{\text{HNO}_3}$ larger than 0.9 for 90% of the time during the haze pollution periods. Therefore, the overall formation rate of particulate nitrate would be determined by the production rate of HNO_3 from the heterogeneous hydrolysis of N_2O_5 and gas-phase $\text{OH} + \text{NO}_2$ reaction. To identify the key chemical factors that controlled the production rates of HNO_3 from these two major reaction pathways, the relationships between the HNO_3 production rate and concentrations of NO_2 and oxidants (i.e., O_3 or OH radicals) are examined and plotted in Figure 10.

As shown in Figure 10a, the slopes of the HNO_3 production rate from the heterogeneous process vs. NO_2 during the nighttime were different under different O_3 concentrations. When O_3 concentrations were higher than 10 ppb, the increase in NO_2 led to a significant increase in HNO_3 production, with the production rate exceeding $5 \mu\text{g m}^{-3} \text{h}^{-1}$ when the NO_2 was higher than 30 ppb. However, when the O_3 level was low (< 10 ppb), the heterogeneous process was relatively slow, even with NO_2 concentration exceeding 60 ppb. These results suggest that the atmospheric oxidation capacity (or the availability of O_3), which affected the production of N_2O_5 , played a vital role in controlling the nitrate formation rate from the heterogeneous process. Furthermore, the reactive uptake of N_2O_5 by aerosols was found to be very efficient (see Figure S10) so that it was not the rate-limiting step of the heterogeneous nitrate formation during the haze pollution periods. Similarly, the slope of the HNO_3 production rate from the gas-phase process vs. NO_2 during the daytime also varied dramatically under different OH radical concentrations (Figure 10b). As the OH radical concentration was higher than $7 \times 10^5 \text{ molecules cm}^{-3}$, this rate increased markedly with the increase in NO_2 . This phenomenon proved again that the atmospheric oxidation capacity played a driving role in the production of HNO_3 from the gas-phase process.

The results in Figure 10 also suggest that solely reducing the NO_x emissions might result in an increase of O_3 and OH concentrations (Lu et al., 2019; Zhao et al., 2020b), which could enhance the oxidation of NO_x and thereby offset the effect of NO_x emission reductions on HNO_3 production. Therefore, a synergistic control of atmospheric oxidant and NO_x emissions would be of great importance for mitigating wintertime particulate nitrate pollution in the eastern YRD.

3.5 Nitrate aerosol formation during the COVID-19

The city lockdowns during the COVID-19 epidemic resulted in substantial emission reductions from vehicular and industrial sources, which provided an opportunity to investigate the response of secondary aerosols to primary emission reductions. Here, we selected the 23 January, 2019 as a

demarcation point (since then many cities in China started to implement lockdown measures) and analyzed the characteristics of particulate nitrate pollution before and during the COVID-19 epidemic.

Figure 11 shows the concentrations of major gaseous and particulate air pollutants, NOR, and sulfur oxidation ratio (SOR) in the eastern YRD before (1-22 January, 2020) and during (23 January-12 February, 2020) the COVID-19 epidemic. At the Pudong site (Figure 11 a, b, c), the average NO_x concentration decreased by 57% due to marked reductions in vehicular emissions during the epidemic. In contrast, the SO_2 concentration only had a small decrease (16%) during the epidemic, since it mainly comes from coal-combustion sources and is less affected by vehicular emissions. However, the O_3 concentration increased by 66% during the epidemic. This is mainly due to the significant reduction in NO_x emissions, though the changes in meteorological conditions could also contribute (Zhao et al., 2020b). Accordingly, the model simulations show that the atmospheric OH concentration (median) increased by 14% during the epidemic, though the average value only increased slightly. The increase in O_3 and OH concentrations could significantly promote the oxidation of NO_x to nitrate and SO_2 to sulfate through both gas-phase and heterogeneous processes. As shown in Figure 11c, the average values of NOR and SOR increased from 0.15 and 0.46 before the epidemic to 0.21 and 0.50 during the epidemic, respectively. The enhanced oxidation of NO_x and SO_2 would weaken the response of particulate nitrate and sulfate to the emission reductions. As can be seen in Figure 11b and c, the simulated HNO_3 production rate and measured particulate nitrate concentration dropped by 42% and 40% during the epidemic, respectively, which were both significantly smaller than the decrease in NO_x concentration (57%), while the particulate sulfate concentration only decreased by 2%, also substantially smaller than the reduction in SO_2 concentration (16%).

Similarly, at the Qingpu site, the NO_x concentration decreased by 58% during the epidemic, while the concentrations of O_3 and OH radicals (median) increased by 90% and 17%, respectively. The significantly enhanced atmospheric oxidation capacity made the simulated HNO_3 production rate only decrease by 17% during the epidemic. However, the measured particulate nitrate concentration at this site decreased by 60%, comparable to the decrease in NO_x concentration. The inconsistency between the decrease in measured nitrate concentration and simulated HNO_3 production rate at the Qingpu site was different from the situation observed at the Pudong site, which is likely due to the fact that the Qingpu site was more easily to be influenced by the regional transport. We note that the average wind speed at the Qingpu site (1.8 m s^{-1}) was higher than that at the Pudong site (1.1 m s^{-1}). Besides, the haze pollution was more serious at the Qingpu site than at the Pudong site before the epidemic: both $\text{PM}_{2.5}$ and nitrate concentrations were significantly higher at the Qingpu site (see Figure 11). Therefore, the marked emission reductions on a regional scale during the epidemic would decrease both the local formation and transport of particulate nitrate from the upwind regions, resulting in a more pronounced reduction in observed nitrate concentration at the Qingpu site. In addition, before the epidemic, the transport of aged air plume with relatively high nitrate and sulfate

concentrations from upwind regions resulted in relatively high NOR and SOR values at the Qingpu site. However, during the epidemic, the significant decrease in nitrate and sulfate concentrations in the aged air plume due to regional emission reductions led to lower NOR and SOR at this site.

The results at the Pudong site clearly show that the enhanced atmospheric oxidation capacity during the COVID-19 epidemic promoted the formation of secondary aerosols and offset the effects of primary emission reductions in the eastern YRD. Such a phenomenon has also been observed in many other regions in China during the COVID-19 lockdown (Le et al., 2020; Zheng et al., 2020; Huang et al., 2021; Liu et al., 2021; Tian et al., 2021; Zhong et al., 2021). These results suggest an important role of atmospheric oxidation capacity in regulating secondary aerosol formation. They also highlight the importance of the synergetic regulation of atmospheric oxidants and other air pollutants in the mitigation of particulate pollution in China. However, the Qingpu site also provided us a special case that in severely polluted regions with a stronger influence from the regional transport, the offset effects of enhanced atmospheric oxidation capacity on emission reductions could be more complicated and less significant.

4. Conclusions

In this study, the chemical mechanisms and key controlling factors of wintertime nitrate formation in the eastern YRD of China were investigated using a combination of online field observations and detailed model simulations. During the observation period (Winter 2018 and 2019), the haze pollution events ($PM_{2.5} > 75 \mu g m^{-3}$) occurred frequently in this region. The mass fraction of nitrate in $PM_{2.5}$ increased dramatically with $PM_{2.5}$ concentration and exceeded 30% throughout the pollution periods. The measured nitrate concentration was well correlated with $[NO_2]^2 \times [O_3]$ (an indicator of N_2O_5) at night and the level of O_x (an indicator of atmospheric oxidation capacity) during the daytime, indicating that both the heterogeneous hydrolysis of N_2O_5 and gas-phase $OH + NO_2$ process played important roles in wintertime nitrate formation in the eastern YRD. Observation-constrained model simulations further show that the average production rates of HNO_3 from the heterogeneous hydrolysis of N_2O_5 during the nighttime and gas-phase $OH + NO_2$ reaction during the daytime were $3.81 \mu g m^{-3} h^{-1}$ and $2.61 \mu g m^{-3} h^{-1}$, respectively, during the haze pollution periods; these two pathways accounted for 66% and 32% of wintertime nitrate formation in the eastern YRD, respectively.

The ALWC significantly promoted the formation of nitrate by facilitating the hydrolysis of N_2O_5 and the gas-to-particle partitioning of HNO_3 . However, the promoting effect of ALWC on nitrate formation varied with aerosol pH due to its significant influence on the gas-to-particle partitioning of HNO_3 . During the pollution periods, the gas-to-particle partitioning of HNO_3 was very efficient, with the partitioning coefficients, ϵ_{HNO_3} , larger than 0.9 for 90% of the time. Therefore, the overall formation processes of wintertime particulate nitrate were not limited by the gas-to-particle partitioning of HNO_3 but rather by its production from both heterogeneous and gas-phase processes. Further analyses of the response of HNO_3 formation to the variation in the concentrations of NO_2 ,

O₃, and OH radicals suggests that the atmospheric oxidation capacity (i.e., the availability of O₃ and OH radicals) played a key role in controlling the formation of nitrate from both processes. During the COVID-19 lockdown (January-February 2020), the enhanced atmospheric oxidation capacity promoted the oxidation of NO_x to nitrate and weaken the effects of primary emission reductions on particulate pollution in typical urban areas in the eastern YRD, though such an offset effect was less significant in regions with a stronger influence from the regional transport. This phenomenon again suggests that the atmospheric oxidation capacity played an important role in driving the formation of secondary aerosols, and highlights the importance of the synergetic regulation of atmospheric oxidation capacity and other air pollutants in the mitigation of particulate pollution in eastern China.

Data availability. The data presented in this work are available upon request from the corresponding authors.

Author contributions. YZ designed the study, JH, QZ, QF, and YD performed field measurements, JYS conducted ISORROPIA-II model calculation, JA and CH provided the NO_x emission inventory, and YZ and HZ analyzed the data, conducted model simulations, and wrote the paper. All other authors contributed to discussion and writing.

Competing interests. The authors declare no conflict of interest.

Acknowledgments. Yue Zhao acknowledges the Program for Professor of Special Appointment (Eastern Scholar) at Shanghai Institutions of Higher Learning. The authors are grateful to Drs. Hongli Wang and Yaqin Gao for kindly sharing their monoterpene observation data for a sensitivity test.

Financial support. This work was supported by the National Natural Science Foundation of China (Grant # 22022607) and the Science and Technology Commission of Shanghai Municipality (Grant # 19DZ1205004).

References:

- Alexander, B., Sherwen, T., Holmes, C. D., Fisher, J. A., Chen, Q., Evans, M. J., and Kasibhatla, P.: Global inorganic nitrate production mechanisms: comparison of a global model with nitrate isotope observations, *Atmos. Chem. Phys.*, 20, 3859-3877, doi: 10.5194/acp-20-3859-2020, 2020.
- [An, J., Huang, Y., Huang, C., Wang, X., Yan, R., Wang, Q., Wang, H., Jing, S. a., Zhang, Y., and Liu, Y.: Emission inventory of air pollutants and chemical speciation for specific anthropogenic sources based on local measurements in the Yangtze River Delta region, China, *Atmos. Chem. Phys.*, 21, 2003-2025, doi, 2021.](#)
- Atkinson, R., and Arey, J.: Atmospheric degradation of volatile organic compounds, *Chem. Rev.*, 103, 4605-4638, doi, 2003.
- Bertram, T. H., and Thornton, J. A.: Toward a general parameterization of N₂O₅ reactivity on aqueous particles: the competing effects of particle liquid water, nitrate and chloride, *Atmos. Chem. Phys.*, 9,

8351-8363, doi, 2009.

Bertram, T. H., Thornton, J. A., Riedel, T. P., Middlebrook, A. M., Bahreini, R., Bates, T. S., Quinn, P. K., and Coffman, D. J.: Direct observations of N_2O_5 reactivity on ambient aerosol particles, *Geophys. Res. Lett.*, 36, doi, 2009.

Brown, S. S., and Stutz, J.: Nighttime radical observations and chemistry, *Chem. Soc. Rev.*, 41, 6405-6447, doi, 2012.

Calvert, J. G., and Stockwell, W. R.: Acid generation in the troposphere by gas-phase chemistry, *Environ. Sci. Technol.*, 17, 428A-443A, doi, 1983.

Chan, Y. C., Evans, M. J., He, P., Holmes, C. D., Jaeglé, L., Kasibhatla, P., Liu, X. Y., Sherwen, T., Thornton, J. A., Wang, X., Xie, Z., Zhai, S., and Alexander, B.: Heterogeneous Nitrate Production Mechanisms in Intense Haze Events in the North China Plain, *J. Geophys. Res.-Atmos.*, 126, doi: 10.1029/2021jd034688, 2021.

Chen, X., Wang, H., Liu, Y., Su, R., Wang, H., Lou, S., and Lu, K.: Spatial characteristics of the nighttime oxidation capacity in the Yangtze River Delta, China, *Atmos. Environ.*, 208, 150-157, doi: 10.1016/j.atmosenv.2019.04.012, 2019.

Chen, X., Wang, H., Lu, K., Li, C., Zhai, T., Tan, Z., Ma, X., Yang, X., Liu, Y., Chen, S., Dong, H., Li, X., Wu, Z., Hu, M., Zeng, L., and Zhang, Y.: Field Determination of Nitrate Formation Pathway in Winter Beijing, *Environ. Sci. Technol.*, 54, 9243-9253, doi: 10.1021/acs.est.0c00972, 2020.

Ding, A., Fu, C., Yang, X., Sun, J., Zheng, L., Xie, Y., Herrmann, E., Nie, W., Petäjä, T., and Kerminen, V.-M.: Ozone and fine particle in the western Yangtze River Delta: an overview of 1 yr data at the SORPES station, *Atmos. Chem. Phys.*, 13, 5813-5830, doi, 2013.

Ding, A., Huang, X., Nie, W., Chi, X., Xu, Z., Zheng, L., Xu, Z., Xie, Y., Qi, X., Shen, Y., Sun, P., Wang, J., Wang, L., Sun, J., Yang, X.-Q., Qin, W., Zhang, X., Cheng, W., Liu, W., Pan, L., and Fu, C.: Significant reduction of $\text{PM}_{2.5}$ in eastern China due to regional-scale emission control: evidence from SORPES in 2011–2018, *Atmos. Chem. Phys.*, 19, 11791-11801, doi: 10.5194/acp-19-11791-2019, 2019.

Duan, J., Huang, R.-J., Li, Y., Chen, Q., Zheng, Y., Chen, Y., Lin, C., Ni, H., Wang, M., Ovadnevaite, J., Ceburnis, D., Chen, C., Worsnop, D. R., Hoffmann, T., O'Dowd, C., and Cao, J.: Summertime and wintertime atmospheric processes of secondary aerosol in Beijing, *Atmos. Chem. Phys.*, 20, 3793-3807, doi: 10.5194/acp-20-3793-2020, 2020.

Fang, Y., Ye, C., Wang, J., Wu, Y., Hu, M., Lin, W., Xu, F., and Zhu, T.: Relative humidity and O_3 concentration as two prerequisites for sulfate formation, *Atmos. Chem. Phys.*, 19, 12295-12307, doi: 10.5194/acp-19-12295-2019, 2019.

Finlayson-Pitts, B. J., Ezell, M. J., and Pitts, J. N.: Formation of chemically active chlorine compounds by reactions of atmospheric NaCl particles with gaseous N_2O_5 and ClONO_2 , *Nature*, 337, 241-244, doi: 10.1038/337241a0, 1989.

Fountoukis, C., and Nenes, A.: ISORROPIA II: a computationally efficient thermodynamic equilibrium model for $\text{K}^+ - \text{Ca}^{2+} - \text{Mg}^{2+} - \text{NH}_4^+ - \text{Na}^+ - \text{SO}_4^{2-} - \text{NO}_3^- - \text{Cl}^- - \text{H}_2\text{O}$ aerosols, *Atmos. Chem. Phys.*, 7, 4639-4659, doi, 2007.

Fu, X., Wang, T., Gao, J., Wang, P., Liu, Y., Wang, S., Zhao, B., and Xue, L.: Persistent Heavy Winter Nitrate Pollution Driven by Increased Photochemical Oxidants in Northern China, *Environ. Sci. Technol.*, 54, 3881-3889, doi: 10.1021/acs.est.9b07248, 2020.

Guo, H., Xu, L., Bougiatioti, A., Cerully, K. M., Capps, S. L., Hite Jr, J., Carlton, A., Lee, S.-H., Bergin, M., and Ng, N.: Fine-particle water and pH in the southeastern United States, *Atmos. Chem. Phys.*, 15, 5211-5228, doi, 2015.

Guo, H., Sullivan, A. P., Campuzano - Jost, P., Schroder, J. C., Lopez - Hilfiker, F. D., Dibb, J. E., Jimenez, J. L., Thornton, J. A., Brown, S. S., and Nenes, A.: Fine particle pH and the partitioning of nitric acid during winter in the northeastern United States, *J. Geophys. Res.-Atmos.*, 121, 10,355-310,376, doi, 2016.

Guo, H., Otjes, R., Schlag, P., Kiendler-Scharr, A., Nenes, A., and Weber, R. J.: Effectiveness of ammonia reduction on control of fine particle nitrate, *Atmos. Chem. Phys.*, 18, 12241-12256, doi, 2018.

Han, C., Yang, W., Wu, Q., Yang, H., and Xue, X.: Heterogeneous photochemical conversion of NO_2 to HONO on the humic acid surface under simulated sunlight, *Environ. Sci. Technol.*, 50, 5017-5023, doi, 2016.

685 He, P., Xie, Z., Chi, X., Yu, X., Fan, S., Kang, H., Liu, C., and Zhan, H.: Atmospheric $\Delta^{17}\text{O}(\text{NO}_3^-)$
686 reveals nocturnal chemistry dominates nitrate production in Beijing haze, *Atmos. Chem. Phys.*, 18,
687 14465-14476, doi: 10.5194/acp-18-14465-2018, 2018.

688 Hennigan, C., Izumi, J., Sullivan, A., Weber, R., and Nenes, A.: A critical evaluation of proxy methods
689 used to estimate the acidity of atmospheric particles, *Atmos. Chem. Phys.*, 15, 2775-2790, doi, 2015.

690 Hua, Y., Cheng, Z., Wang, S., Jiang, J., Chen, D., Cai, S., Fu, X., Fu, Q., Chen, C., and Xu, B.:
691 Characteristics and source apportionment of $\text{PM}_{2.5}$ during a fall heavy haze episode in the Yangtze
692 River Delta of China, *Atmos. Environ.*, 123, 380-391, doi, 2015.

693 Huang, R.-J., He, Y., Duan, J., Li, Y., Chen, Q., Zheng, Y., Chen, Y., Hu, W., Lin, C., and Ni, H.:
694 Contrasting sources and processes of particulate species in haze days with low and high relative
695 humidity in wintertime Beijing, *Atmos. Chem. Phys.*, 20, 9101-9114, doi, 2020.

696 Huang, R. J., Zhang, Y. L., Bozzetti, C., Ho, K. F., Cao, J. J., Han, Y. M., Daellenbach, K. R., Slowik, J.
697 G., Platt, S. M., Canonaco, F., Zotter, P., Wolf, R., Pieber, S. M., Bruns, E. A., Crippa, M., Ciarelli,
698 G., Piazzalunga, A., Schwikowski, M., Abbaszade, G., Schnelle-Kreis, J., Zimmermann, R., An, Z.
699 S., Szidat, S., Baltensperger, U., El Haddad, I., and Prevot, A. S. H.: High secondary aerosol
700 contribution to particulate pollution during haze events in China, *Nature*, 514, 218-222, doi, 2014.

701 Huang, X., Ding, A., Gao, J., Zheng, B., Zhou, D., Qi, X., Tang, R., Wang, J., Ren, C., and Nie, W.:
702 Enhanced secondary pollution offset reduction of primary emissions during COVID-19 lockdown in
703 China, *Natl. Sci. Rev.*, 8, nwaa137, doi, 2021.

704 Jenkin, M., Young, J., and Rickard, A.: The MCM v3.3.1 degradation scheme for isoprene, *Atmos.*
705 *Chem. Phys.*, 15, 11433-11459, doi, 2015.

706 Kleffmann, J., Becker, K., and Wiesen, P.: Heterogeneous NO_2 conversion processes on acid surfaces:
707 possible atmospheric implications, *Atmos. Environ.*, 32, 2721-2729, doi, 1998.

708 Kong, L., Yang, Y., Zhang, S., Zhao, X., Du, H., Fu, H., Zhang, S., Cheng, T., Yang, X., and Chen, J.:
709 Observations of linear dependence between sulfate and nitrate in atmospheric particles, *J. Geophys.*
710 *Res.-Atmos.*, 119, 341-361, doi, 2014.

711 Kong, L., Feng, M., Liu, Y., Zhang, Y., Zhang, C., Li, C., Qu, Y., An, J., Liu, X., Tan, Q., Cheng, N.,
712 Deng, Y., Zhai, R., and Wang, Z.: Elucidating the pollution characteristics of nitrate, sulfate and
713 ammonium in $\text{PM}_{2.5}$ in Chengdu, southwest China, based on 3-year measurements, *Atmos. Chem.*
714 *Phys.*, 20, 11181-11199, doi: 10.5194/acp-20-11181-2020, 2020.

715 Kurtenbach, R., Becker, K., Gomes, J., Kleffmann, J., Lörzer, J., Spittler, M., Wiesen, P., Ackermann,
716 R., Geyer, A., and Platt, U.: Investigations of emissions and heterogeneous formation of HONO in a
717 road traffic tunnel, *Atmos. Environ.*, 35, 3385-3394, doi, 2001.

718 Le, T., Wang, Y., Liu, L., Yang, J., Yung, Y. L., Li, G., and Seinfeld, J. H.: Unexpected air pollution
719 with marked emission reductions during the COVID-19 outbreak in China, *Science*, 369, 702-706,
720 doi, 2020.

721 Lee, Y., and Schwartz, S. E.: Kinetics of oxidation of aqueous sulfur (IV) by nitrogen dioxide,
722 Precipitation Scavenging, Dry Deposition and Resuspension, 1, 453-470, doi, 1983.

723 Lelieveld, J., Evans, J. S., Fnais, M., Giannadaki, D., and Pozzer, A.: The contribution of outdoor air
724 pollution sources to premature mortality on a global scale, *Nature*, 525, 367-+, doi, 2015.

725 Li, H., Zhang, Q., Zheng, B., Chen, C., Wu, N., Guo, H., Zhang, Y., Zheng, Y., Li, X., and He, K.:
726 Nitrate-driven urban haze pollution during summertime over the North China Plain, *Atmos. Chem.*
727 *Phys.*, 18, 5293-5306, doi: 10.5194/acp-18-5293-2018, 2018.

728 Li, H., Cheng, J., Zhang, Q., Zheng, B., Zhang, Y., Zheng, G., and He, K.: Rapid transition in winter
729 aerosol composition in Beijing from 2014 to 2017: response to clean air actions, *Atmos. Chem.*
730 *Phys.*, 19, 11485-11499, doi, 2019a.

731 Li, K., Jacob, D. J., Liao, H., Zhu, J., Shah, V., Shen, L., Bates, K. H., Zhang, Q., and Zhai, S.: A two-
732 pollutant strategy for improving ozone and particulate air quality in China, *Nat. Geosci.*, 12, 906-
733 910, doi, 2019b.

734 Li, M., Wang, T., Xie, M., Li, S., Zhuang, B., Huang, X., Chen, P., Zhao, M., and Liu, J.: Formation
735 and evolution mechanisms for two extreme haze episodes in the Yangtze River Delta region of China
736 during winter 2016, *J. Geophys. Res.-Atmos.*, 124, 3607-3623, doi, 2019c.

737 Lin, Y.-C., Zhang, Y.-L., Fan, M.-Y., and Bao, M.: Heterogeneous formation of particulate nitrate under
738 ammonium-rich regimes during the high- $\text{PM}_{2.5}$ events in Nanjing, China, *Atmos. Chem. Phys.*, 20,
739 3999-4011, doi: 10.5194/acp-20-3999-2020, 2020.

- Liu, L., Zhang, J., Du, R., Teng, X., Hu, R., Yuan, Q., Tang, S., Ren, C., Huang, X., and Xu, L.: Chemistry of atmospheric fine particles during the COVID-19 pandemic in a megacity of Eastern China, *Geophys. Res. Lett.*, 48, 2020GL091611, doi, 2021.
- Liu, P., Ye, C., Xue, C., Zhang, C., Mu, Y., and Sun, X.: Formation mechanisms of atmospheric nitrate and sulfate during the winter haze pollution periods in Beijing: gas-phase, heterogeneous and aqueous-phase chemistry, *Atmos. Chem. Phys.*, 20, 4153-4165, doi: 10.5194/acp-20-4153-2020, 2020a.
- Liu, Y., Lu, K., Ma, Y., Yang, X., Zhang, W., Wu, Y., Peng, J., Shuai, S., Hu, M., and Zhang, Y.: Direct emission of nitrous acid (HONO) from gasoline cars in China determined by vehicle chassis dynamometer experiments, *Atmos. Environ.*, 169, 89-96, doi, 2017.
- Liu, Y., Lu, K., Li, X., Dong, H., Tan, Z., Wang, H., Zou, Q., Wu, Y., Zeng, L., Hu, M., Min, K. E., Kecorius, S., Wiedensohler, A., and Zhang, Y.: A Comprehensive Model Test of the HONO Sources Constrained to Field Measurements at Rural North China Plain, *Environ. Sci. Technol.*, 53, 3517-3525, doi: 10.1021/acs.est.8b06367, 2019.
- Liu, Y., and Wang, T.: Worsening urban ozone pollution in China from 2013 to 2017–Part 1: The complex and varying roles of meteorology, *Atmos. Chem. Phys.*, 20, 6305-6321, doi, 2020.
- Liu, Y. C., Zhang, Y. S., Lian, C. F., Yan, C., Feng, Z. M., Zheng, F. X., Fan, X. L., Chen, Y., Wang, W. G., Chu, B. W., Wang, Y. H., Cai, J., Du, W., Daellenbach, K. R., Kangasluoma, J., Bianchi, F., Kujansuu, J., Petaja, T., Wang, X. F., Hu, B., Wang, Y. S., Ge, M. F., He, H., and Kulmala, M.: The promotion effect of nitrous acid on aerosol formation in wintertime in Beijing: the possible contribution of traffic-related emissions, *Atmos. Chem. Phys.*, 20, 13023-13040, doi: 10.5194/acp-20-13023-2020, 2020b.
- Lu, K. D., Fuchs, H., Hofzumahaus, A., Tan, Z. F., Wang, H. C., Zhang, L., Schmitt, S. H., Rohrer, F., Bohn, B., Broch, S., Dong, H. B., Gkatzelis, G. I., Hohaus, T., Holland, F., Li, X., Liu, Y., Liu, Y. H., Ma, X. F., Novelli, A., Schlag, P., Shao, M., Wu, Y. S., Wu, Z. J., Zeng, L. M., Hu, M., Kiendler-Scharr, A., Wahner, A., and Zhang, Y. H.: Fast Photochemistry in Wintertime Haze: Consequences for Pollution Mitigation Strategies, *Environ. Sci. Technol.*, 53, 10676-10684, doi: 10.1021/acs.est.9b02422, 2019.
- Lu, X., Hong, J., Zhang, L., Cooper, O. R., Schultz, M. G., Xu, X., Wang, T., Gao, M., Zhao, Y., and Zhang, Y.: Severe surface ozone pollution in China: a global perspective, *Environ. Sci. Technol. Lett.*, 5, 487-494, doi, 2018.
- McDuffie, E. E., Womack, C. C., Fibiger, D. L., Dube, W. P., Franchin, A., Middlebrook, A. M., Goldberger, L., Lee, B., Thornton, J. A., Moravek, A., Murphy, J. G., Baasandorj, M., and Brown, S. S.: On the contribution of nocturnal heterogeneous reactive nitrogen chemistry to particulate matter formation during wintertime pollution events in Northern Utah, *Atmos. Chem. Phys.*, 19, 9287-9308, doi: 10.5194/acp-19-9287-2019, 2019.
- Mozurkewich, M., and Calvert, J. G.: Reaction probability of N_2O_5 on aqueous aerosols, *J. Geophys. Res.-Atmos.*, 93, 15889-15896, doi, 1988.
- Peng, J. F., Hu, M., Shang, D. J., Wu, Z. J., Du, Z. F., Tan, T. Y., Wang, Y. N., Zhang, F., and Zhang, R. Y.: Explosive Secondary Aerosol Formation during Severe Haze in the North China Plain, *Environ. Sci. Technol.*, 55, 2189-2207, doi: 10.1021/acs.est.0c07204, 2021.
- Romer, P. S., Wooldridge, P. J., Crounse, J. D., Kim, M. J., Wennberg, P. O., Dibb, J. E., Scheuer, E., Blake, D. R., Meinardi, S., and Brosius, A. L.: Constraints on Aerosol Nitrate Photolysis as a Potential Source of HONO and NO_x , *Environ. Sci. Technol.*, 52, 13738-13746, doi, 2018.
- Schweitzer, F., Mirabel, P., and George, C.: Multiphase chemistry of N_2O_5 , $ClNO_2$, and $BrNO_2$, *J. Phys. Chem. A*, 102, 3942-3952, doi: DOI 10.1021/jp980748s, 1998.
- Shao, P. Y., Tian, H. Z., Sun, Y. J., Liu, H. J., Wu, B. B., Liu, S. H., Liu, X. Y., Wu, Y. M., Liang, W. Z., Wang, Y., Gao, J. J., Xue, Y. F., Bai, X. X., Liu, W., Lin, S. M., and Hu, G. Z.: Characterizing remarkable changes of severe haze events and chemical compositions in multi-size airborne particles (PM_1 , $PM_{2.5}$ and PM_{10}) from January 2013 to 2016-2017 winter in Beijing, China, *Atmos. Environ.*, 189, 133-144, doi: 10.1016/j.atmosenv.2018.06.038, 2018.
- Shen, J., Zhao, Q., Cheng, Z., Wang, P., Ying, Q., Liu, J., Duan, Y., and Fu, Q.: Insights into source origins and formation mechanisms of nitrate during winter haze episodes in the Yangtze River Delta, *Sci. Total. Environ.*, 741, 140187, doi: 10.1016/j.scitotenv.2020.140187, 2020.
- Slater, E. J., Whalley, L. K., Woodward-Massey, R., Ye, C., Lee, J. D., Squires, F., Hopkins, J. R., Dunmore, R. E., Shaw, M., and Hamilton, J. F.: Elevated levels of OH observed in haze events

during wintertime in central Beijing, *Atmos. Chem. Phys.*, 20, 14847-14871, doi, 2020.

Su, X., Tie, X., Li, G., Cao, J., Huang, R., Feng, T., Long, X., and Xu, R.: Effect of hydrolysis of N_2O_5 on nitrate and ammonium formation in Beijing China: WRF-Chem model simulation, *Sci. Total Environ.*, 579, 221-229, doi, 2017.

Sun, P., Nie, W., Chi, X., Xie, Y., Huang, X., Xu, Z., Qi, X., Xu, Z., Wang, L., Wang, T., Zhang, Q., and Ding, A.: Two years of online measurement of fine particulate nitrate in the western Yangtze River Delta: influences of thermodynamics and N_2O_5 hydrolysis, *Atmos. Chem. Phys.*, 18, 17177-17190, doi: 10.5194/acp-18-17177-2018, 2018.

Tan, Z., Fuchs, H., Lu, K., Hofzumahaus, A., Bohn, B., Broch, S., Dong, H., Gomm, S., Häsel, R., and He, L.: Radical chemistry at a rural site (Wangdu) in the North China Plain: observation and model calculations of OH, HO_2 and RO_2 radicals, *Atmos. Chem. Phys.*, 17, 663-690, doi, 2017.

Tao, J., Zhang, L. M., Cao, J. J., and Zhang, R. J.: A review of current knowledge concerning $\text{PM}_{2.5}$ chemical composition, aerosol optical properties and their relationships across China, *Atmos. Chem. Phys.*, 17, 9485-9518, doi: 10.5194/acp-17-9485-2017, 2017.

Tao, Y., Ye, X., Ma, Z., Xie, Y., Wang, R., Chen, J., Yang, X., and Jiang, S.: Insights into different nitrate formation mechanisms from seasonal variations of secondary inorganic aerosols in Shanghai, *Atmos. Environ.*, 145, 1-9, doi: 10.1016/j.atmosenv.2016.09.012, 2016.

Thornton, J. A., and Abbatt, J. P. D.: N_2O_5 reaction on submicron sea salt aerosol: Kinetics, products, and the effect of surface active organics, *J. Phys. Chem. A*, 109, 10004-10012, doi: 10.1021/jp054183t, 2005.

Tian, J., Wang, Q., Zhang, Y., Yan, M., Liu, H., Zhang, N., Ran, W., and Cao, J.: Impacts of primary emissions and secondary aerosol formation on air pollution in an urban area of China during the COVID-19 lockdown, *Environ. Int.*, 150, 106426, doi, 2021.

Trinh, H. T., Imanishi, K., Morikawa, T., Hagino, H., and Takenaka, N.: Gaseous nitrous acid (HONO) and nitrogen oxides (NO_x) emission from gasoline and diesel vehicles under real-world driving test cycles, *J. Air. Waste. Manage.*, 67, 412-420, doi, 2017.

von Schneidmesser, E., Monks, P. S., Allan, J. D., Bruhwiler, L., Forster, P., Fowler, D., Lauer, A., Morgan, W. T., Paasonen, P., Righi, M., Sindelarova, K., and Sutton, M. A.: Chemistry and the Linkages between Air Quality and Climate Change, *Chem. Rev.*, 115, 3856-3897, doi: 10.1021/acs.chemrev.5b00089, 2015.

Wagner, N., Riedel, T., Young, C., Bahreini, R., Brock, C., Dubé, W., Kim, S., Middlebrook, A., Öztürk, F., and Roberts, J.: N_2O_5 uptake coefficients and nocturnal NO_2 removal rates determined from ambient wintertime measurements, *J. Geophys. Res.-Atmos.*, 118, 9331-9350, doi, 2013.

Wang, H., Lu, K., Chen, X., Zhu, Q., Chen, Q., Guo, S., Jiang, M., Li, X., Shang, D., Tan, Z., Wu, Y., Wu, Z., Zou, Q., Zheng, Y., Zeng, L., Zhu, T., Hu, M., and Zhang, Y.: High N_2O_5 Concentrations Observed in Urban Beijing: Implications of a Large Nitrate Formation Pathway, *Environ. Sci. Technol. Lett.*, 4, 416-420, doi: 10.1021/acs.estlett.7b00341, 2017.

Wang, J., Li, J., Ye, J., Zhao, J., Wu, Y., Hu, J., Liu, D., Nie, D., Shen, F., Huang, X., Huang, D. D., Ji, D., Sun, X., Xu, W., Guo, J., Song, S., Qin, Y., Liu, P., Turner, J. R., Lee, H. C., Hwang, S., Liao, H., Martin, S. T., Zhang, Q., Chen, M., Sun, Y., Ge, X., and Jacob, D. J.: Fast sulfate formation from oxidation of SO_2 by NO_2 and HONO observed in Beijing haze, *Nat. Commun.*, 11, 2844, doi: 10.1038/s41467-020-16683-x, 2020a.

Wang, W., Yu, J., Cui, Y., He, J., Xue, P., Cao, W., Ying, H., Gao, W., Yan, Y., Hu, B., Xin, J., Wang, L., Liu, Z., Sun, Y., Ji, D., and Wang, Y.: Characteristics of fine particulate matter and its sources in an industrialized coastal city, Ningbo, Yangtze River Delta, China, *Atmos. Res.*, 203, 105-117, doi: 10.1016/j.atmosres.2017.11.033, 2018.

Wang, Y., Zhang, R., and Saravanan, R.: Asian pollution climatically modulates mid-latitude cyclones following hierarchical modelling and observational analysis, *Nat. Commun.*, 5, 1-7, doi, 2014.

Wang, Y., Chen, Y., Wu, Z., Shang, D., Bian, Y., Du, Z., Schmitt, S. H., Su, R., Gkatzelis, G. I., Schlag, P., Hohaus, T., Voliotis, A., Lu, K., Zeng, L., Zhao, C., Alfarra, M. R., McFiggans, G., Wiedensohler, A., Kiendler-Scharr, A., Zhang, Y., and Hu, M.: Mutual promotion between aerosol particle liquid water and particulate nitrate enhancement leads to severe nitrate-dominated particulate matter pollution and low visibility, *Atmos. Chem. Phys.*, 20, 2161-2175, doi: 10.5194/acp-20-2161-2020, 2020b.

Wayne, R. P., Barnes, I., Biggs, P., Burrows, J., Canosa-Mas, C., Hjorth, J., Le Bras, G., Moortgat, G., Perner, D., and Poulet, G.: The nitrate radical: Physics, chemistry, and the atmosphere, *Atmos.*

Environ.. Part A. General Topics, 25, 1-203, doi, 1991.

Wen, L., Chen, J., Yang, L., Wang, X., Xu, C., Sui, X., Yao, L., Zhu, Y., Zhang, J., and Zhu, T.: Enhanced formation of fine particulate nitrate at a rural site on the North China Plain in summer: The important roles of ammonia and ozone, *Atmos. Environ.*, 101, 294-302, doi, 2015.

Wen, L., Xue, L., Wang, X., Xu, C., Chen, T., Yang, L., Wang, T., Zhang, Q., and Wang, W.: Summertime fine particulate nitrate pollution in the North China Plain: increasing trends, formation mechanisms and implications for control policy, *Atmos. Chem. Phys.*, 18, 11261-11275, doi: 10.5194/acp-18-11261-2018, 2018.

Wolfe, G. M., Marvin, M. R., Roberts, S. J., Travis, K. R., and Liao, J.: The framework for 0-D atmospheric modeling (F0AM) v3.1, *Geosci. Model. Dev.*, 9, 3309-3319, doi, 2016.

Wong, K., Oh, H.-J., Lefer, B., Rappenglück, B., and Stutz, J.: Vertical profiles of nitrous acid in the nocturnal urban atmosphere of Houston, TX, *Atmos. Chem. Phys.*, 11, 3595-3609, doi, 2011.

Wong, K., Tsai, C., Lefer, B., Grossberg, N., and Stutz, J.: Modeling of daytime HONO vertical gradients during SHARP 2009, *Atmos. Chem. Phys.*, 13, 3587-3601, doi, 2013.

Xie, Y., Ding, A., Nie, W., Mao, H., Qi, X., Huang, X., Xu, Z., Kerminen, V. M., Petäjä, T., and Chi, X.: Enhanced sulfate formation by nitrogen dioxide: Implications from in situ observations at the SORPES station, *J. Geophys. Res.-Atmos.*, 120, 12679-12694, doi, 2015.

Xie, Y., Wang, G., Wang, X., Chen, J., Chen, Y., Tang, G., Wang, L., Ge, S., Xue, G., Wang, Y., and Gao, J.: Nitrate-dominated PM_{2.5} and elevation of particle pH observed in urban Beijing during the winter of 2017, *Atmos. Chem. Phys.*, 20, 5019-5033, doi: 10.5194/acp-20-5019-2020, 2020.

Xu, Q., Wang, S., Jiang, J., Bhattarai, N., Li, X., Chang, X., Qiu, X., Zheng, M., Hua, Y., and Hao, J.: Nitrate dominates the chemical composition of PM_{2.5} during haze event in Beijing, China, *Sci. Total. Environ.*, 689, 1293-1303, doi, 2019.

Xue, C., Zhang, C., Ye, C., Liu, P., Catoire, V., Krysztofiak, G., Chen, H., Ren, Y., Zhao, X., Wang, J., Zhang, F., Zhang, C., Zhang, J., An, J., Wang, T., Chen, J., Kleffmann, J., Mellouki, A., and Mu, Y.: HONO Budget and Its Role in Nitrate Formation in the Rural North China Plain, *Environ. Sci. Technol.*, 54, 11048-11057, doi: 10.1021/acs.est.0c01832, 2020.

Yang, G., Liu, Y., and Li, X.: Spatiotemporal distribution of ground-level ozone in China at a city level, *Sci. Rep.*, 10, 1-12, doi, 2020.

Ye, C., Zhou, X., Pu, D., Stutz, J., Festa, J., Spolaor, M., Tsai, C., Cantrell, C., Mauldin, R. L., and Campos, T.: Rapid cycling of reactive nitrogen in the marine boundary layer, *Nature*, 532, 489-491, doi, 2016.

Ye, S., Ma, T., Duan, F., Li, H., He, K., Xia, J., Yang, S., Zhu, L., Ma, Y., and Huang, T.: Characteristics and formation mechanisms of winter haze in Changzhou, a highly polluted industrial city in the Yangtze River Delta, China, *Environ. Pollut.*, 253, 377-383, doi, 2019.

Ye, Z., Liu, J., Gu, A., Feng, F., Liu, Y., Bi, C., Xu, J., Li, L., Chen, H., Chen, Y., Dai, L., Zhou, Q., and Ge, X.: Chemical characterization of fine particulate matter in Changzhou, China, and source apportionment with offline aerosol mass spectrometry, *Atmos. Chem. Phys.*, 17, 2573-2592, doi: 10.5194/acp-17-2573-2017, 2017.

Yu, C., Wang, Z., Xia, M., Fu, X., Wang, W., Tham, Y. J., Chen, T., Zheng, P., Li, H., Shan, Y., Wang, X., Xue, L., Zhou, Y., Yue, D., Ou, Y., Gao, J., Lu, K., Brown, S. S., Zhang, Y., and Wang, T.: Heterogeneous N₂O₅ reactions on atmospheric aerosols at four Chinese sites: improving model representation of uptake parameters, *Atmos. Chem. Phys.*, 20, 4367-4378, doi: 10.5194/acp-20-4367-2020, 2020a.

Yu, Y., Xu, H., Jiang, Y., Chen, F., and Liu, D.: A modeling study of PM_{2.5} transboundary transport during a winter severe haze episode in southern Yangtze River Delta, China, *Atmos. Res.*, 248, 105159, doi, 2020b.

Yun, H., Wang, W., Wang, T., Xia, M., Yu, C., Wang, Z., Poon, S. C., Yue, D., and Zhou, Y.: Nitrate formation from heterogeneous uptake of dinitrogen pentoxide during a severe winter haze in southern China, *Atmos. Chem. Phys.*, 18, 17515-17527, doi, 2018.

Zare, A., Romer, P. S., Nguyen, T., Keutsch, F. N., Skog, K., and Cohen, R. C.: A comprehensive organic nitrate chemistry: insights into the lifetime of atmospheric organic nitrates, *Atmos. Chem. Phys.*, 18, 15419-15436, doi: 10.5194/acp-18-15419-2018, 2018.

Zhai, S., Jacob, D. J., Wang, X., Liu, Z., Wen, T., Shah, V., Li, K., Moch, J. M., Bates, K. H., Song, S., Shen, L., Zhang, Y., Luo, G., Yu, F., Sun, Y., Wang, L., Qi, M., Tao, J., Gui, K., Xu, H., Zhang, Q.,

- Zhao, T., Wang, Y., Lee, H. C., Choi, H., and Liao, H.: Control of particulate nitrate air pollution in China, *Nat. Geosci.*, 14, 389-395, doi: 10.1038/s41561-021-00726-z, 2021.
- Zhang, Q., Zheng, Y. X., Tong, D., Shao, M., Wang, S. X., Zhang, Y. H., Xu, X. D., Wang, J. N., He, H., Liu, W. Q., Ding, Y. H., Lei, Y., Li, J. H., Wang, Z. F., Zhang, X. Y., Wang, Y. S., Cheng, J., Liu, Y., Shi, Q. R., Yan, L., Geng, G. N., Hong, C. P., Li, M., Liu, F., Zheng, B., Cao, J. J., Ding, A. J., Gao, J., Fu, Q. Y., Huo, J. T., Liu, B. X., Liu, Z. R., Yang, F. M., He, K. B., and Hao, J. M.: Drivers of improved PM_{2.5} air quality in China from 2013 to 2017, *Proc. Natl. Acad. Sci. U.S.A.*, 116, 24463-24469, doi: 10.1073/pnas.1907956116, 2019.
- Zhang, T., Shen, Z., Su, H., Liu, S., Zhou, J., Zhao, Z., Wang, Q., Prévôt, A., and Cao, J.: Effects of Aerosol Water Content on the formation of secondary inorganic aerosol during a Winter Heavy PM_{2.5} Pollution Episode in Xi'an, China, *Atmos. Environ.*, 252, 118304, doi, 2021.
- Zhang, Y.-L., and Cao, F.: Fine particulate matter (PM_{2.5}) in China at a city level, *Sci. Rep.*, 5, 1-12, doi, 2015.
- Zhao, P., Dong, F., He, D., Zhao, X., Zhang, X., Zhang, W., Yao, Q., and Liu, H.: Characteristics of concentrations and chemical compositions for PM_{2.5} in the region of Beijing, Tianjin, and Hebei, China, *Atmos. Chem. Phys.*, 13, 4631-4644, doi, 2013.
- Zhao, Q., Huo, J., Yang, X., Fu, Q., Duan, Y., Liu, Y., Lin, Y., and Zhang, Q.: Chemical characterization and source identification of submicron aerosols from a year-long real-time observation at a rural site of Shanghai using an Aerosol Chemical Speciation Monitor, *Atmos. Res.*, 246, doi: 10.1016/j.atmosres.2020.105154, 2020a.
- Zhao, Y. B., Zhang, K., Xu, X. T., Shen, H. Z., Zhu, X., Zhang, Y. X., Hu, Y. T., and Shen, G. F.: Substantial Changes in Nitrogen Dioxide and Ozone after Excluding Meteorological Impacts during the COVID-19 Outbreak in Mainland China, *Environ. Sci. Technol. Lett.*, 7, 402-408, doi, 2020b.
- Zheng, B., Tong, D., Li, M., Liu, F., Hong, C. P., Geng, G. N., Li, H. Y., Li, X., Peng, L. Q., Qi, J., Yan, L., Zhang, Y. X., Zhao, H. Y., Zheng, Y. X., He, K. B., and Zhang, Q.: Trends in China's anthropogenic emissions since 2010 as the consequence of clean air actions, *Atmos. Chem. Phys.*, 18, 14095-14111, doi: 10.5194/acp-18-14095-2018, 2018.
- Zheng, H., Kong, S., Chen, N., Yan, Y., Liu, D., Zhu, B., Xu, K., Cao, W., Ding, Q., Lan, B., Zhang, Z., Zheng, M., Fan, Z., Cheng, Y., Zheng, S., Yao, L., Bai, Y., Zhao, T., and Qi, S.: Significant changes in the chemical compositions and sources of PM_{2.5} in Wuhan since the city lockdown as COVID-19, *Sci. Total. Environ.*, 739, 140000, doi: 10.1016/j.scitotenv.2020.140000, 2020.
- Zhong, H., Huang, R.-J., Chang, Y., Duan, J., Lin, C., and Chen, Y.: Enhanced formation of secondary organic aerosol from photochemical oxidation during the COVID-19 lockdown in a background site in Northwest China, *Sci. Total. Environ.*, 778, 144947, doi, 2021.

943 Table 1 Parameterization of the formation and removal pathways of HONO added to the model.

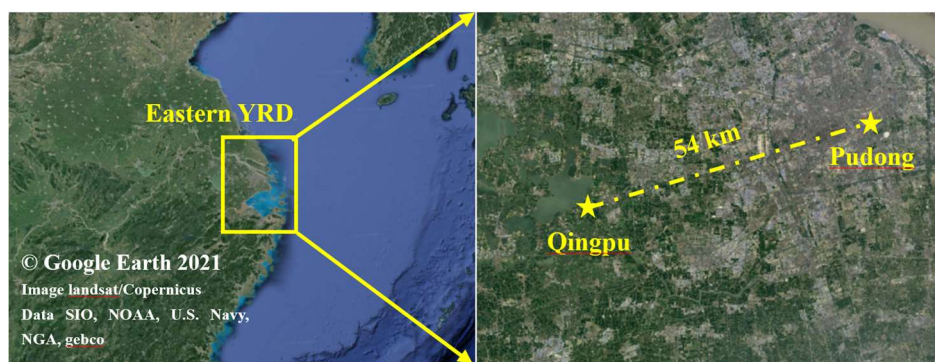
Mechanism	Parametrization	Max	Min	Ref
$\text{NO}_2 + \text{aerosol} \rightarrow 0.5\text{HONO} + 0.5\text{HNO}_3$	$\gamma\text{NO}_2 = 2 \times 10^{-6}$	1×10^{-5}	4×10^{-7}	a-d
$\text{NO}_2 + \text{ground} \rightarrow \text{HONO}$	$\gamma\text{NO}_2 = 2 \times 10^{-6}$	1×10^{-5}	4×10^{-7}	a-d
$\text{NO}_2 + \text{aerosol} + h\nu \rightarrow \text{HONO}$	$\gamma\text{NO}_2 = 2 \times 10^{-5} \times j\text{NO}_2 / j\text{NO}_2\text{noon}^*$	1×10^{-4}	4×10^{-6}	b, e-g
$\text{NO}_2 + \text{ground} + h\nu \rightarrow \text{HONO}$	$\gamma\text{NO}_2 = 2 \times 10^{-5} \times j\text{NO}_2 / j\text{NO}_2\text{noon}^*$	1×10^{-4}	4×10^{-6}	b, e-g
$\text{pNO}_3 + h\nu \rightarrow \text{HONO}$	$j\text{NO}_3 = j\text{HNO}_3 \times 30$	100	1	h, i
Vehicular emission	$\text{HONO}/\text{NO}_x = 0.8\%$	0.18%	1.6%	j-l
$\text{NO}_2 + \text{SO}_2 + \text{aerosol} \rightarrow \text{HONO} + \text{SO}_4^{2-}$	$k_{aq} = 1.4 \times 10^5 \text{ M}^{-1} \text{ s}^{-1}$ (pH < 5); $2 \times 10^6 \text{ M}^{-1} \text{ s}^{-1}$ (pH > 6)			m, n
	$v_{\text{HONO}} (\text{m s}^{-1}) = \exp^{(23920/T-91.5)}$			a
HONO deposition	$k_{\text{dep}} (\text{s}^{-1}) = \exp^{(23920/T-91.5)} v_{\text{HONO}} / \text{PBL} (\text{m})$			

944 *The value of $j\text{NO}_2\text{noon}$ used in the model was 0.005 s^{-1} ; References: ^aXue et al. (2020); ^bLiu et al.
945 (2019); ^cWong et al. (2011); ^dKleffmann et al. (1998); ^eWong et al. (2013); ^fZare et al. (2018); ^gHan
946 et al. (2016); ^hRomer et al. (2018); ⁱYe et al. (2016); ^jKurtenbach et al. (2001); ^kLiu et al. (2017),
947 ^lTrinh et al. (2017); ^mLee and Schwartz (1983); ⁿWang et al. (2020a).

951 Table 2 Concentrations (average \pm standard deviation) of $\text{PM}_{2.5}$, particulate nitrate, NO_x , and O_3 , as
952 well as temperature and RH at Qingpu and Pudong sites in the winter of 2018 and 2019.

	Sites			
	Qingpu-2018	Pudong-2018	Qingpu-2019	Pudong-2019
$\text{PM}_{2.5}$ ($\mu\text{g m}^{-3}$)	50.0 ± 34.8	40.9 ± 32.5	58.6 ± 37.2	49.5 ± 35.3
NO_3^- ($\mu\text{g m}^{-3}$)	14.9 ± 12.8	11.9 ± 12.2	17.0 ± 14.8	13.2 ± 12.0
NO_x (ppb)	29.6 ± 31.1	27.5 ± 24.4	35.1 ± 33.1	26.9 ± 21.3
O_3 (ppb)	19.1 ± 12.7	18.8 ± 10.4	21.7 ± 14.3	22.3 ± 12.0
Temperature ($^{\circ}\text{C}$)	6.6 ± 4.4	7.3 ± 4.2	7.5 ± 4.2	8.2 ± 3.8
RH (%)	80 ± 17	78 ± 18	80 ± 17	79 ± 20

955



956

957 Figure 1 Map of the eastern YRD region and the two observation sites, i.e., Qingpu (suburban and
958 regional) and Pudong (urban).

959

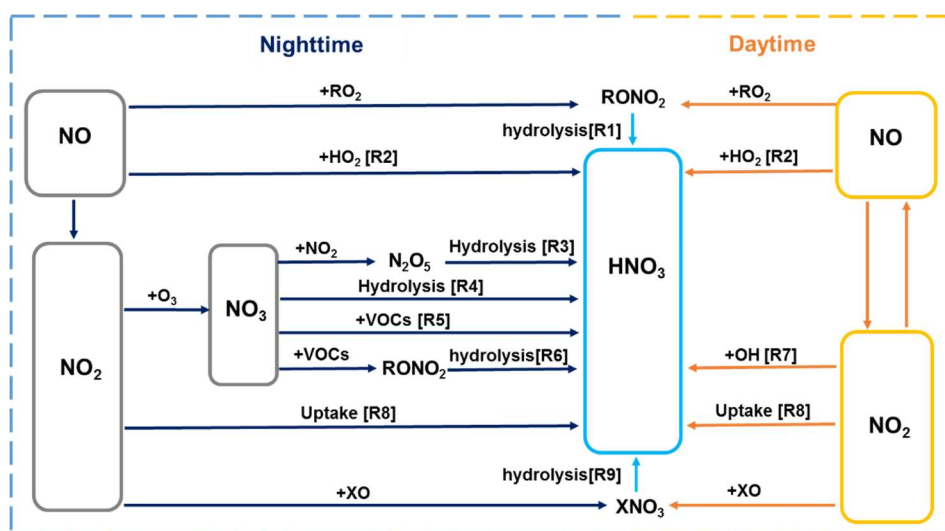


Figure 2 Simplified HNO_3 formation mechanisms in the troposphere. X represents Cl, Br, and I.

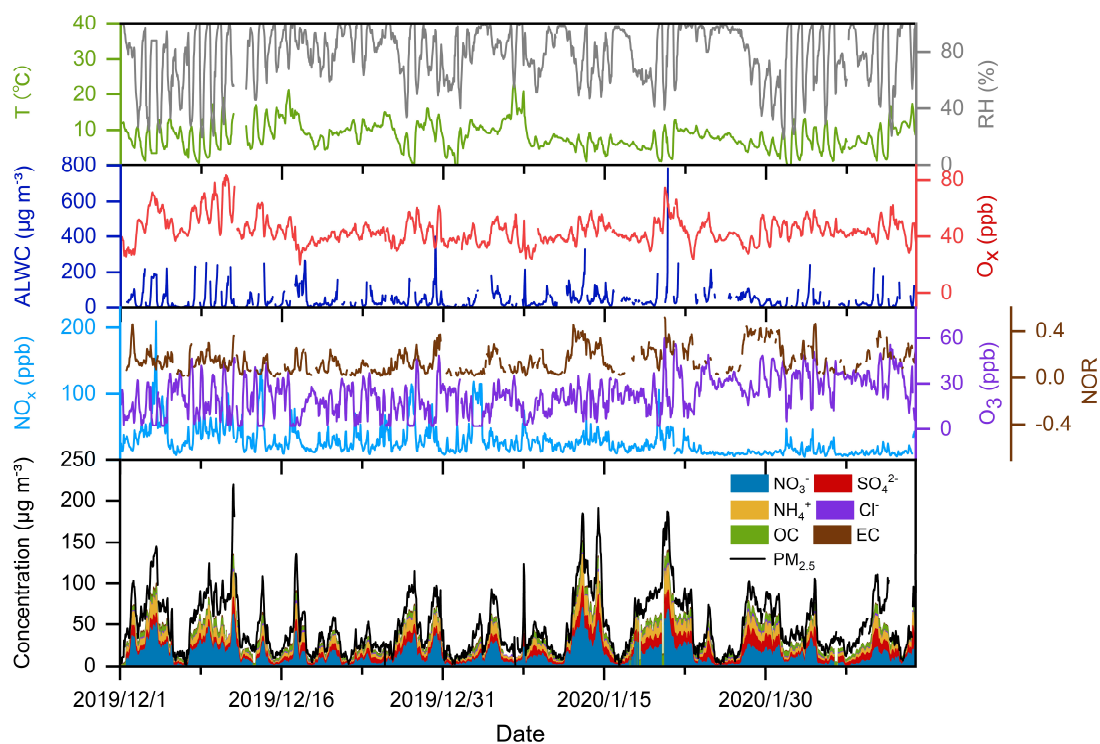


Figure 3 Time series of temperature, relative humidity (RH), aerosol liquid water content (ALWC), NO_x , O_3 , O_x , nitrogen oxidation ratio (NOR), as well as $\text{PM}_{2.5}$ and major particulate compositions at the Pudong site in the winter of 2019.

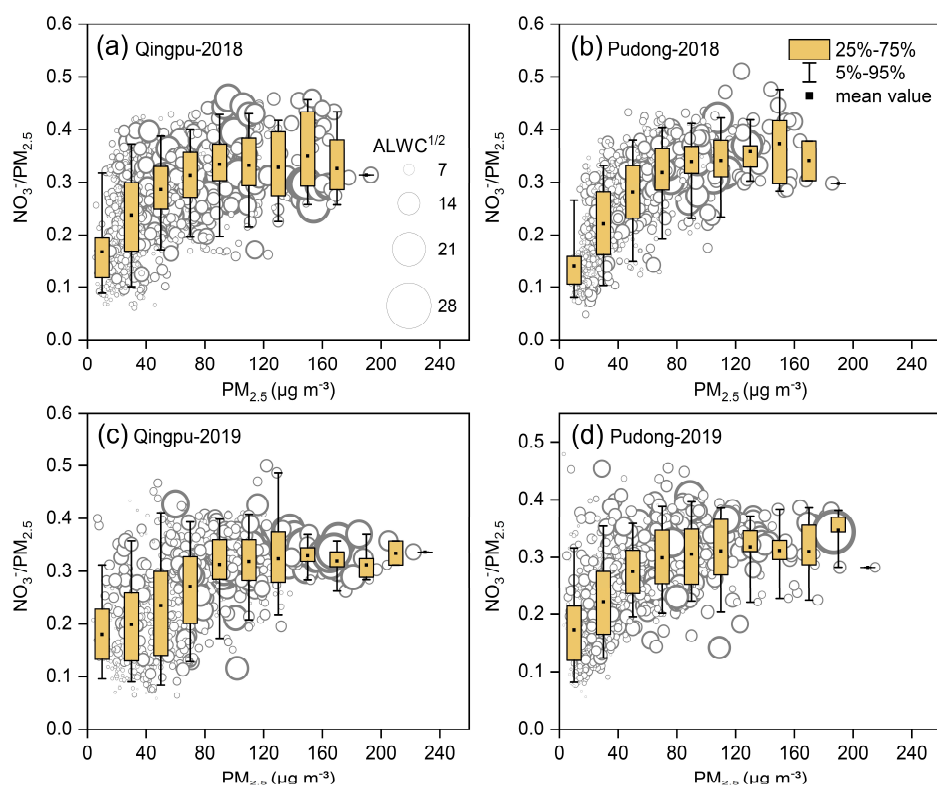


Figure 4 Mass ratio of nitrate to $PM_{2.5}$ as a function of $PM_{2.5}$ concentration at (a, c) Qingpu and (b, d) Pudong sites in the winter of 2018 and 2019. The circles represent the measured ratio of $NO_3^-/PM_{2.5}$, and their area is linearly scaled with square root of ALWC.

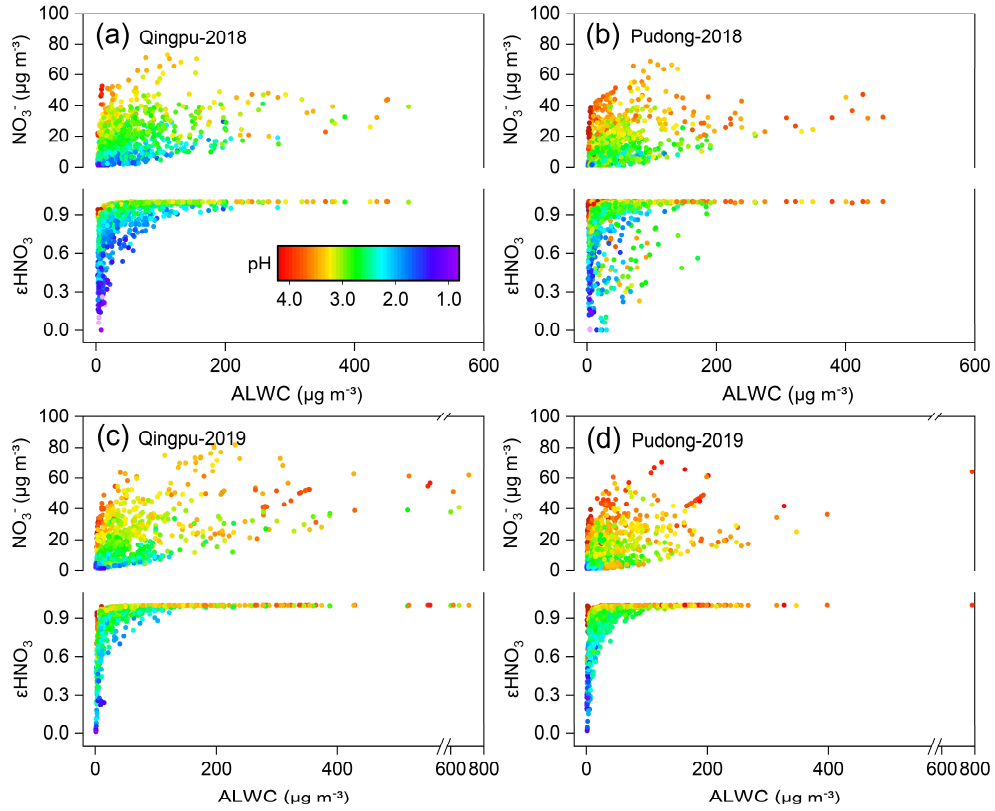


Figure 5 Particulate nitrate concentration and its fraction to total nitrate (ϵHNO_3) as a function of ALWC and aerosol pH at (a, c) Qingpu and (b, d) Pudong sites in the winter of 2018 and 2019. The circles are colored according to aerosol pH.

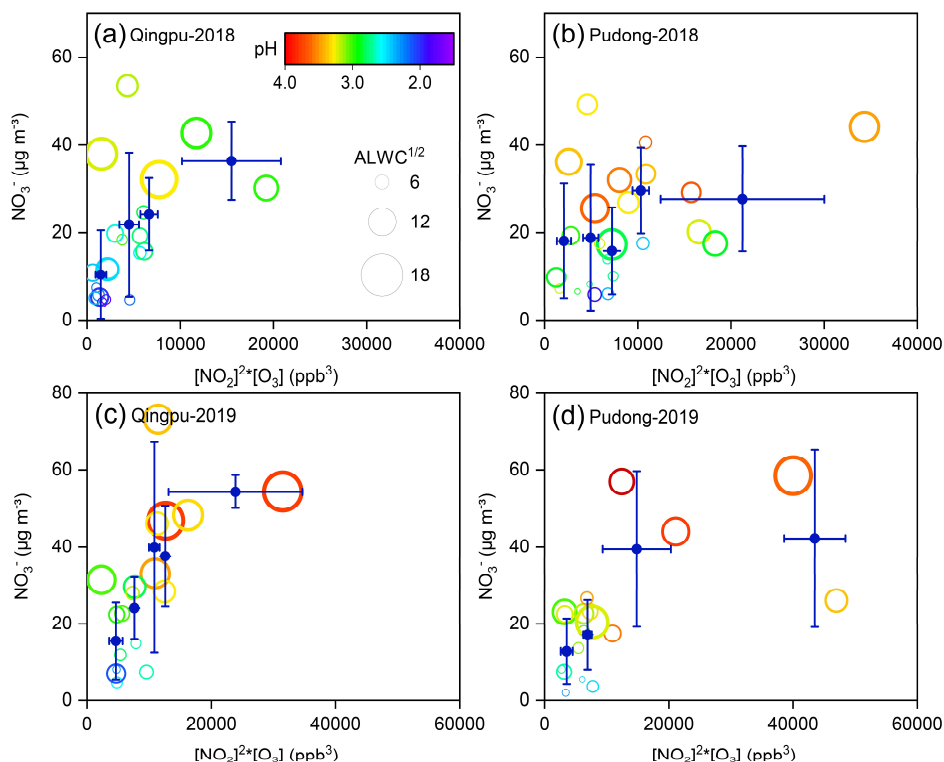


Figure 6 Nighttime average particulate nitrate concentration (empty circles) as a function of $[\text{NO}_2]^2 \times [\text{O}_3]$ at (a, c) Qingpu and (b, d) Pudong sites in 2018 and 2019. The circles are colored according to aerosol pH and their size is linearly scaled with square root of ALWC. The blue filled circles represent the average of nitrate concentration within a certain $[\text{NO}_2]^2 \times [\text{O}_3]$ interval. To reduce the influences of daytime remainder on the analysis of nighttime nitrate formation, only the data with an obvious peak or increasing trend during nighttime were included in the plots.

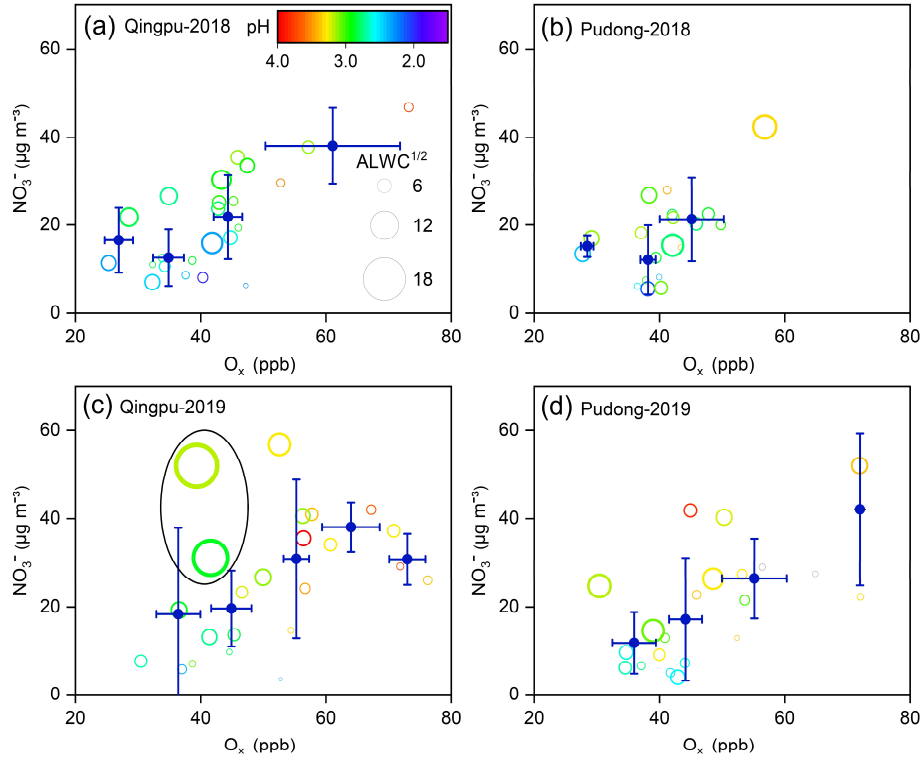


Figure 7 Daytime average particulate nitrate concentration as a function of O_x at (a, c) Qingpu and (b, d) Pudong sites in 2018 and 2019. The circles are colored according to aerosol pH and their size is linearly scaled with square root of ALWC. The blue filled circles represent the average of nitrate concentration within a certain O_x interval. The data points inside the black circle in (c) correspond to low O_x levels but high ALWC and nitrate concentrations. Only the data with an obvious peak or increasing trend during daytime were included in the plots.

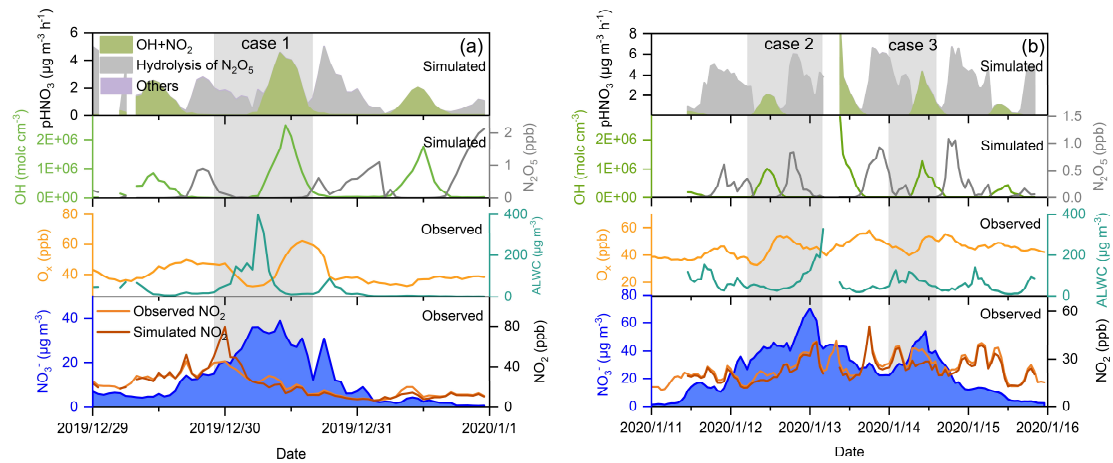


Figure 8 Time series of particulate nitrate, NO_2 , O_3 , ALWC, OH, N_2O_5 , as well as the formation rate of HNO_3 from different processes during the two selected case during the pollution episodes at the Pudong site in 2019. The simulated data with $\text{RH} > 95\%$ were not included in the figure (see main text).

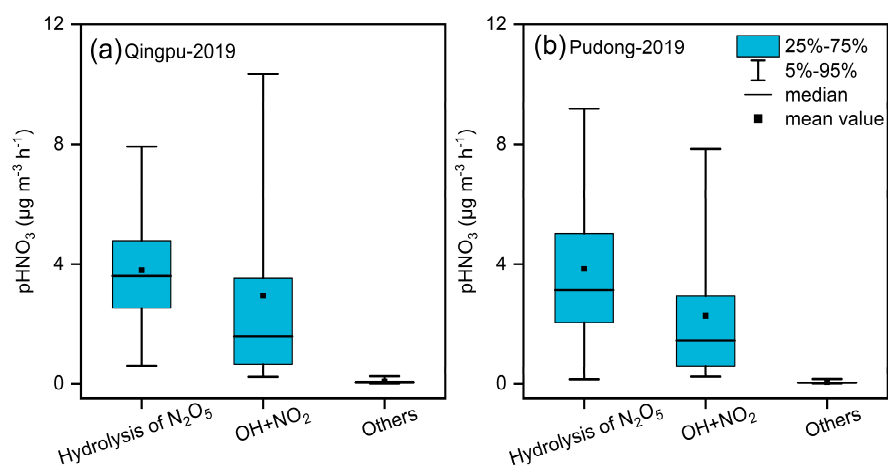


Figure 9 Simulated average formation rates of HNO_3 at (a) Qingpu and (b) Pudong sites during the haze pollution periods in 2019

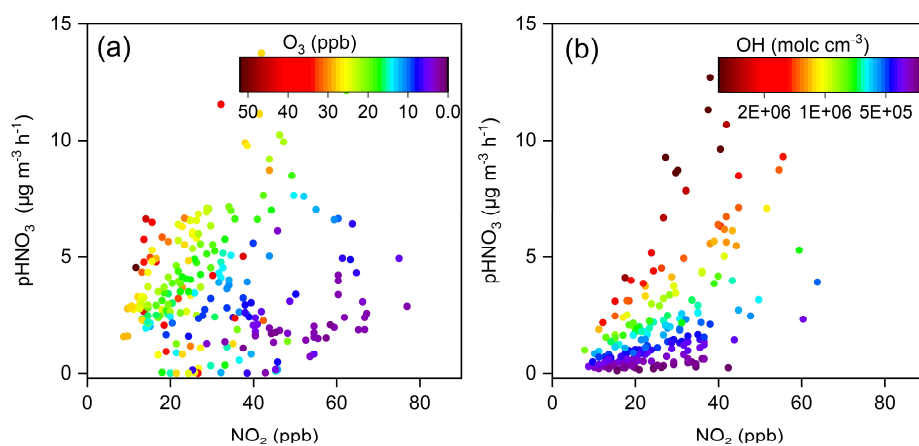


Figure 10 Production rates of HNO_3 from the (a) heterogeneous and (b) gas-phase processes as a function of NO_2 concentration at the Pudong site during the nighttime and daytime, respectively. The circles are colored according to the O_3 concentration in (a) and OH radical concentration in (b).

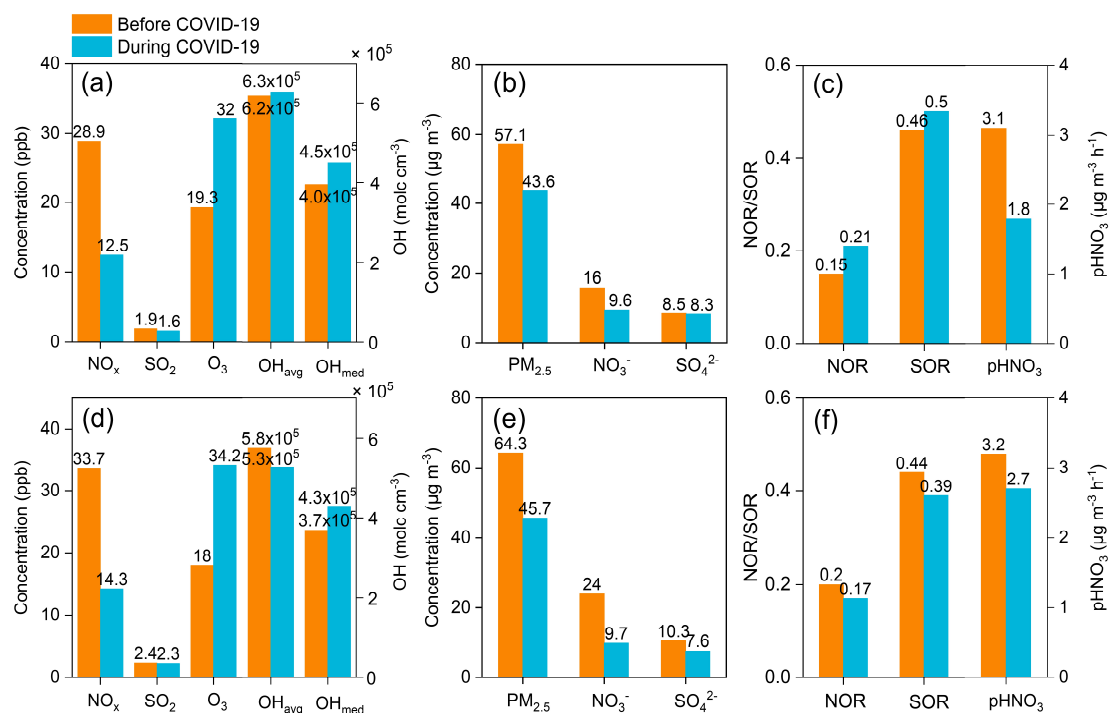


Figure 11 Average concentrations of NO_x, SO₂, O₃, OH radicals, PM_{2.5}, nitrate, sulfate, as well as the nitrogen and sulfur oxidation ratio (NOR and SOR) at (a-c) Pudong and (d-f) Qingpu sites before (1-22 January, 2020) and during (23 January-12 February, 2020) the COVID-19 epidemic.